CZECH TECHNICAL UNIVERSITY

Faculty of Electrical Engineering

Electromagnetic Field Department

Non-Line of Sight Visible Light Communication

Study program: Communication, Multimedia and Electronics

Thesis supervisor: Prof. Ing. Stanislav Zvánovec, Ph.D

<div align="right">

Bc. Ezgi Ertunç

</div>

Prague 2018

MASTER'S THESIS ASSIGNMENT

I. Personal and study details

Student's name:	**Ertunç Ezgi**
Faculty / Institute:	**Faculty of Electrical Engineering**
Department / Institute:	**Department of Circuit Theory**
Study program:	**Communications, Multimedia, Electronics**
Branch of study:	**Systems of Communication**

Personal ID number: **464300**

II. Master's thesis details

Master's thesis title in English:

Non-line of Sight Visible Light Communications

Master's thesis title in Czech:

Non-line of Sight Visible Light Communications

Guidelines:

Recent development in solid-state lighting and highly efficient white light-emitting diodes (LEDs) allowed new communication approach ? Visible Light Communications (VLC). Data rates in the orders of Gb/s over a very short transmission span can be achieved over line-of-sight (LOS) VLC links. Even though indoor VLC can be established by the LOS connections, when the link is shadowed it can use diffuse reflections and communicate via non-LOS (NLOS) path. The main task in the diploma thesis will be to analyticaly and experimentaly analyse utilization of NLOS VLC. Derive optical channel impulse responses using ray-tracing model and analyse experimentally BER performance in case of VLC link with reflection from different surfaces.
Supervisor specialist: Ing. Petr Chvojka

Bibliography / sources:

[1] Z. Ghassemlooy, L. Nero Alves, S. Zvanovec and M. Ali Khalighi, Visible Light Communications: Theory and Applications, CRC Press, 2017.
[2] P. Chvojka, S. Vitek, S. Zvanovec, Z. Ghassemlooy, S. Rajbhandari, Analyses of Non-Line of Sight Visible Light Communications, Optical Engineering, vol. 56, no.11, pp. 116116-1 - 7, 2017.

Name and workplace of master's thesis supervisor:

prof. Ing. Stanislav Zvánovec, Ph.D.,   Department of Electromagnetic Field,   FEL

Name and workplace of second master's thesis supervisor or consultant:

Date of master's thesis assignment: **26.02.2018**   Deadline for master's thesis submission: _____

Assignment valid until: **30.09.2019**

prof. Ing. Stanislav Zvánovec, Ph.D. Supervisor's signature	prof. Ing. Pavel Sovka, CSc. Head of department's signature	prof. Ing. Pavel Ripka, CSc. Dean's signature

III. Assignment receipt

The student acknowledges that the master's thesis is an individual work. The student must produce her thesis without the assistance of others, with the exception of provided consultations. Within the master's thesis, the author must state the names of consultants and include a list of references.

Date of assignment receipt	Student's signature

Decleration

I hereby declare that the master thesis at hand is my own written work and I also confirm that I have only used the specified resources which are identified in the references.

In Prague on 15th August 2018

....

Bc. Ezgi Ertunc

ACKNOWLEDGEMENT

ABSTRACT

Recent development in solid-state lighting and highly efficient white light-emitting diodes (LEDs) allowed new communication approach Visible Light Communications (VLC). Data rates in the orders of Gb/s over a very short transmission span can be achieved over line-of-sight (LOS) VLC links. Even though indoor VLC can be established by the LOS connections, when the link is shadowed it can use diffuse reflections and communicate via non-LOS (NLOS) path. This diploma thesis provides to analytically and experimentally analyze utilization of NLOS VLC. The goal is to derive optical channel impulse responses using ray-tracing model and analyze experimentally BER performance in case of VLC link with reflection from different surfaces.

CONTENTS

ABBREVIATION

BER	Bit error rate
BRDF	Bidirectional reflectance distribution function
CIR	Channel impulse response
CP	Cyclic prefix
DC	Direct current
FFT	Fast Fourier transform
FIR	Finite impulse response
FOV	Field of view
ICI	Inter-carrier interference
IFFT	Inverse fast Fourier transform
IM/DD	Intensity modulation//direct detection
LED	Light emitting diode
LOS	Line-of-sıght
m-CAP	Carrierless amplitude and phase modulation
MMCA	Modified Monte Carlo ray tracing
NLOS	Non-line-of-sight
NRZ	Non-return-to-zero
OFDM	Orthogonal frequency division multiplexing
OOK	On-off keying
OWC	Optical wireless communication
P/S	Parallel-to-serial
PAM	Pulse amplitude modulation
PDF	Probability density function
PPM	Pulse position modulation
QAM	Quadrature amplitude modulation
RLS	Recursive least square
RRC	Root raise cosine
S/P	Serial-to-parallel
VLC	Visible light communication

INTRODUCTION

The diploma thesis comprises the fundamental principles underlying visible light communication (VLC) which part of Optical Wireless Communication (OWC). The main idea behind the employment of VLC involves the use of light emitting diodes (LEDs) for transmitting the visible light spectrum ray for both illumination of place and high-speed communication [1].

Measurement part will be completed to non line-of-sight (NLOS) VLC indoor environment in the optical laboratory. In the measurement, calculation of bit error rate (BER) will be observed on the white paper based on different distance of between transmitter-material and receiver-material and different angle of transmitter and angle of receiver will be showned.

Simulation part will be completed using Monte Carlo ray tracing NLOS VLC in indoor environment via MATLAB. Empty rectangular and homogenous walls are assumed. Device-to-device communication is provided by IR link.

Recent wireless mobile data traffic has been growing majorly.As the number of rapidly emerging smart devices (tablets,smartphones,TVs etc.) are which excists radio frequency (RF) spectrum resourses, increases significantly. Hence,researchers have been focusing on to overcome for next-generation wireless communication area [1-2]. Visible light communication (VLC) is an optical wireless communication (OWC) technology that emerging technology for future high capacity communication links is the visible range of the electromagnetic spectrum (~370–780 nm) as indicated visible light spectrum in the Fig. 1 below.
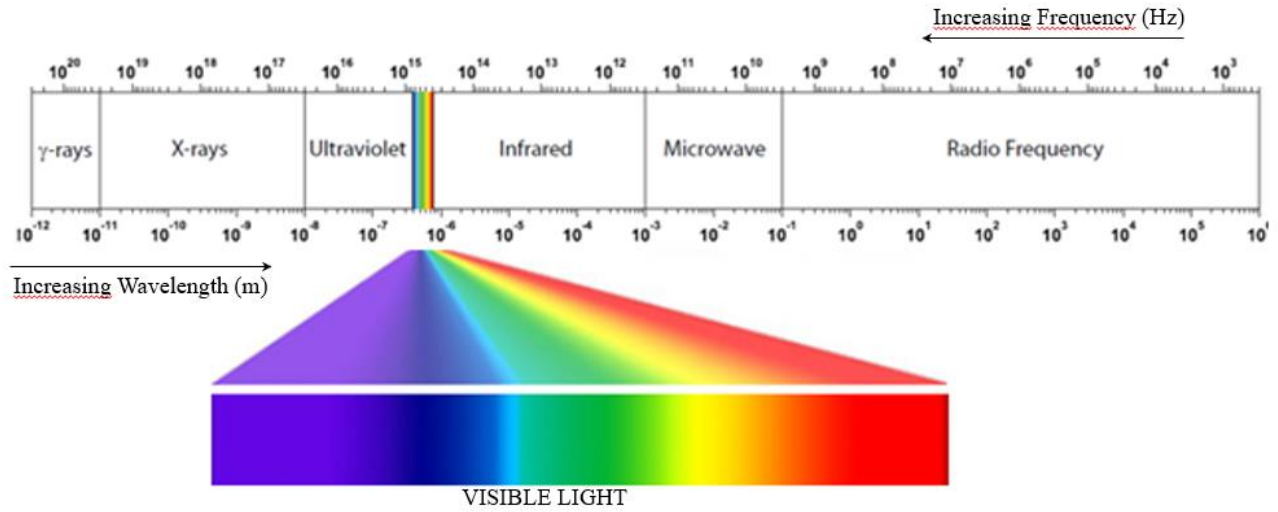
Fig. 1: Electromagnetic spectrum with the marked visible light.

TABLE 1: Properties of visible ligh communication technology adopted from [3]

Property	VLC
Bandwidth	Limited
Electromagnetic Interference	No
Hazard	No
Line of sight	Yes
Security	Good
Standards	IEEE 802.15.7 in progress
Services	Illumication/ambient light
Power consumption	Low
Mobility	Limited
FOV	Limited
Communication range	Short
Covarege	Indoor

1. Visible Light Communication

1.1. Principle of VLC

In this chapter, the basic principle of VLC will be described from transmitter through an optical channel and receiver based on its block diagram.

1.1.1. Transmitter

As such, the LED can then carry out the dual purpose of lighting homes while at the same time transmit high-speed data in the form of modulated light. The next step is for the receiver to convert the optical signal to an electrical signal with the use of a photodiode which recovers the information that had changed format during transmission [4]. With the recent surge in the popularity of VLC as an indoor communication system with wireless properties, this can prove worthwhile if an LED serves as the material of transmission. The reason is that it can transmit modulated data at high speeds as compared to other conventional sources of light [5].

A block diagram of a basic VLC link is illustrated in Fig. 2 which individually shows every part of the system. Firstly, input data is generated and the modulation is applied. There are two types of modulation techniques which most frequently used in the optical communication systems : digital and analog baseband modulation techniques and advanced modulation techniques as shown Fig. 3. The most popular modulations of baseband are on-off keying (OOK), pulse position modulation (PPM), pulse amplitute modulation [1]. The orthagonal frequency division multiplexing which is one of the advanced modulation technique, utilize the bandwidth and phase modulation (CAP) is one of the significant subcarrier modulation.
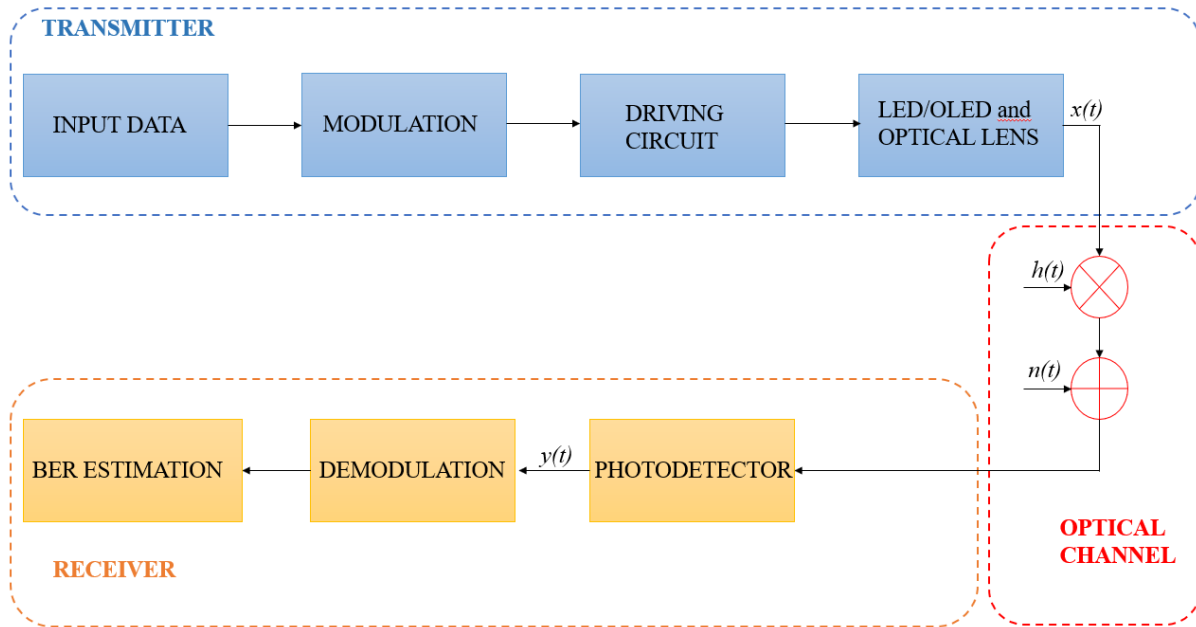
Fig. 2: The block diagram of basic VLC system.
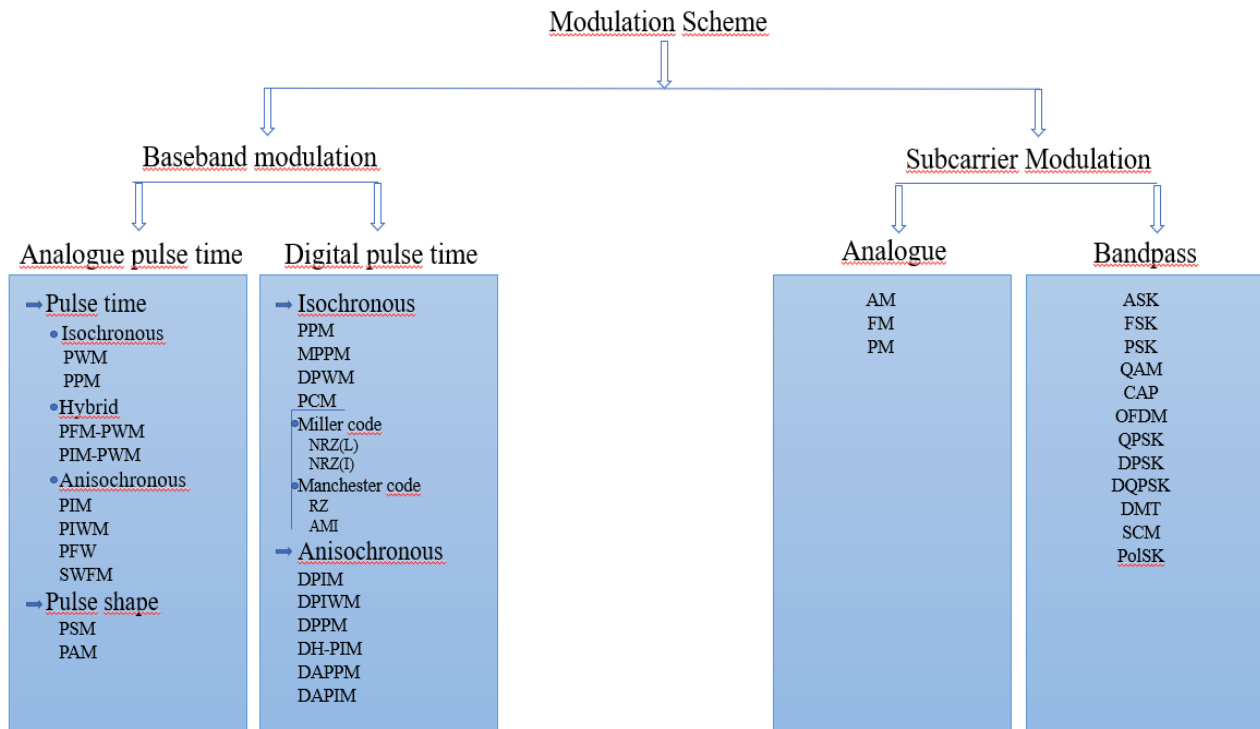
Fig 3: Modulation techniques of optical communication

1.1.1 Receiver

Optical receiver obtains information from transmitter. The receiver (photodetector) must receive information via visible light. Its size is significant in this period. Larger receiver would convert more optical signal into electrical signal. They have a very high sensitivity since she signal is pretty weak after the optical channel [1,2].

1.1.3 Modulation Techniques

1.1.3.1 Baseband Modulation Techniques

The most frequently used modulation is OOK since it is simplest technique to implement and from the point of power efficiency for IM/DD in optical communication. OOK modulation has reported transmission speed of hundreds of Mb/s [6-10]. The other modulation technique is pulse position modulation (PPM) that is significant for dimming control in high power and spectral efficiency as reported in [11-14]. Pulse width modulation (PWM)is used for brightness of the light emitting diode (LED). It is adopted for increasing the efficiency of the tranmission. Pulse amplitude modulation (PAM)provides high bandwidth efficiency in low power efficiency of LEDs as reported [15-17].

Modulation Type	Bandwidth Efficiency	Power Efficiency	SNR	Cost
Digital	Low	High	High	High
OOK-NRZ	R_B	P	Moderate	Low
OOK-RZ	$2R_B$	P-3	Moderate	Low
PPM	$R_b\,L/\log_2 L$	$P- 5\log 10[(L/2)\log_2 L]$	Low	Moderate

Table 2. Comparisons of different baseband modulation techniques.

 OOK-NRZ is the most popular modulation format for VLC as reported [8,18-21].
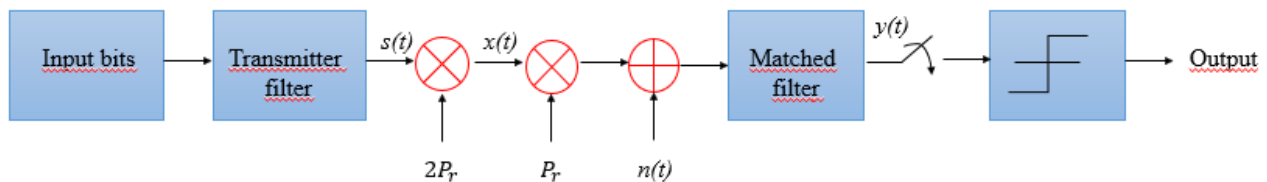
Fig. 4: The block diagram of OOK

In Fig. 4 Transmitter filter has a unit rectangular impulse response. The filter is proportionated by photocurrent $2P_r$ and average received optical power is P_r. $n(t)$ is a shot noise that is added as a Gaussian White noise.

1.1.3.2. Subcarrier Modulation Techniques

Recently, researchers have been focusing the advanced modulation formats such as OFDM and CAP [1,2]. These modulation techniques have been supporting higher order modulation formats such as quadrature amplitude modulation (QAM) to increase the link capacity mostly in bandlimited enviroments. The OFDM technique has been the most popular modulation technique employed due to its compatibility providing out-of-band transmission over hundreds of MHz as reported in [22-29]. Inverse fast Fourier transform (IFFT) in transmitter and fast Fourier (FFT) in receiver utilize to implement the OFDM scheme. The block diagram of OFDM modulation is shown in Fig. 5. It is depicted from [27]. At the transmitter part, input data streams are generated and after the a serial-to-parallel (S/P) conversion, mapped into M-ary QAM (M-QAM) constellation. IFFT tehnique utilizes as multiplexing and modulation and both inter-symbol interference (ISI) and inter-carrier interference (ICI) is reduced by added cyclic prefix (CP) at the beginning of every symbol. LED is modulated before parallel-to-serial (P/S) conversion, At the receeiver part, firstly, CP is removed before S/P conversion. FFT utilizes demodulation and demultiplexing. The received bits are estimated before P/S conversion.
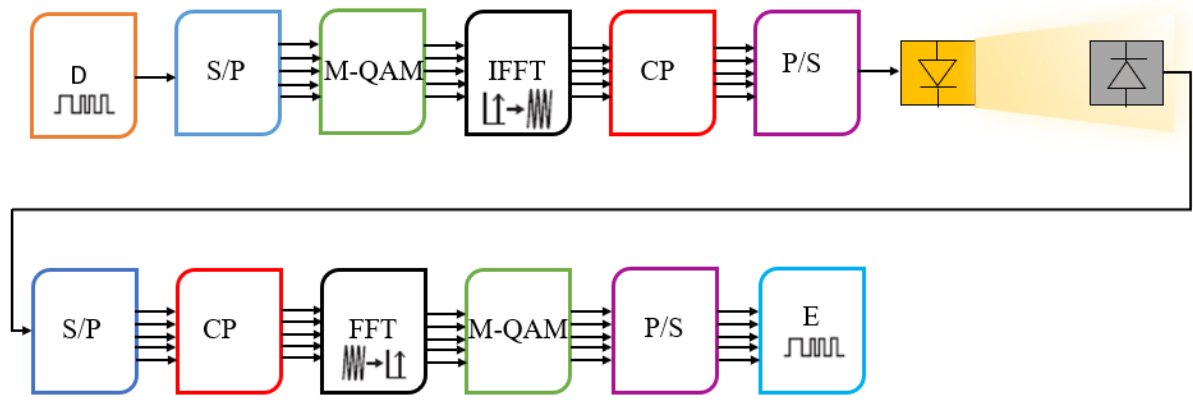
Fig. 5: OFDM block diagram [30].

Carrierless amplitude and phase modulation (m-CAP) is an alternative modulation to OFDM which has many very useful features over OFDM. As [31] reported , the main reason is to use finite impulse response (FIR) for pulse shaping in CAP. Besides,It does not require both IFFT/FFT as OFDM extremly requires. Researchers are already accomplished that CAP modulation format has better achievement than OFDM in VLC as 3.22 Gb/s and 2.93 Gb/s respectively [32,33].

The m-CAP schematic block diagram Fig. 5 is depicted in [30]. After the input data is generated, it is modulated into the constellation. The signal is upsampled, real and imaginary parts are separated into two parts and passed through the pulse shaping transmit filters. The output signal *s(t)* is generated as a sum of M-QAM bits. M is the order of QAM. Then it is used to modulate an LED. After the signal is detected matched filtering is used as time reversal. Finally, the signal is down-sampled and de-modulated, the received bits are estimated.

The transmitted CAP signal *s(t)* is formulated :

$$s(t) = \sum_{n=-\infty}^{\infty} |a_n p(t - nT) - b_n \dot{p}(t - nT) \tag{1}$$

Where T is the symbol period and n is the symbol index, a_n is real part of upsampled symbols and b_n is imaginary part of upsampled symbols.

$$p(t) = g(t)\cos(\omega_c t) \text{ and } \dot{p}(t) = g(t)\sin(\omega_c t) \tag{2}$$

Where *g(t)* is the root raise cosine (RRC) filter, $\omega_c = 2\pi f_c$ and f_c is a sinusoid frequency.

1.2.   Channel Modelling

There are two types of link configurations on VLC: directed line-of-sight (LOS), nondirected LOS (NLOS) as shown Fig. 6.

(a)   (b)

Fig. 6: Link Configuration on VLC. (a) is LOS and (b) is NLOS, T is a transmitter and R is a receiver.

1.2.1.   Line-of-sight (LOS) VLC

In the VLC, it is significant to transfer data from transmitter to receiver. The light propagates through the direct or no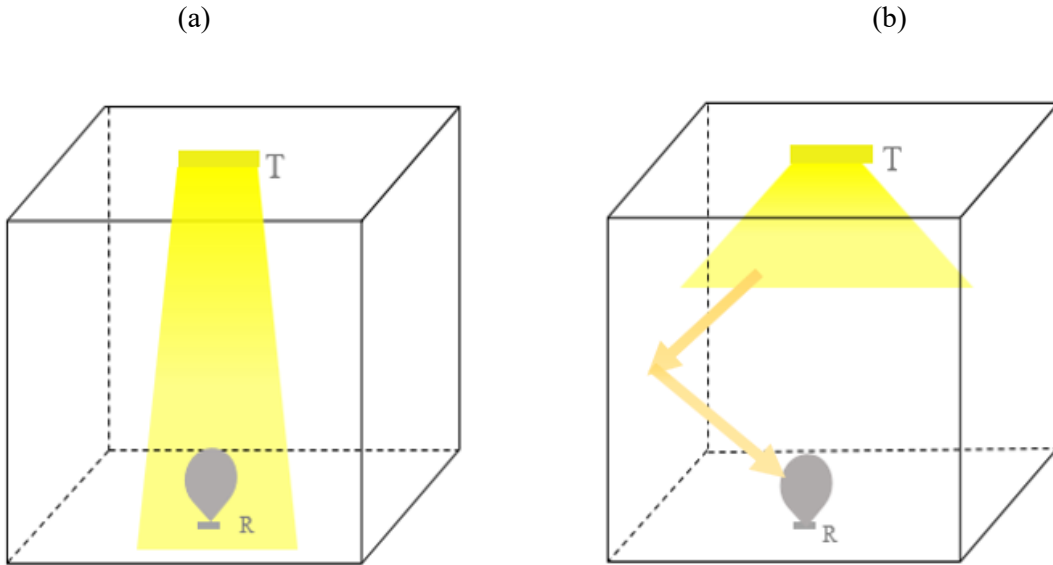n-direct way into the photodetector. Thus, data is obtained by this way. There is a LOS connection in both directed and nondirected between transmitter and receiver. The photodetector collects optical signals and converts into electrical signal. The light distribution is generalised Lambertian radiant intensity as given [1].

$$R_0(\phi) = \begin{cases} \dfrac{(m_1 + 1)}{2\pi} \cos^{m_1}(\phi) & \in [-\pi/2, \pi/2] \\ 0 & \phi \leq \pi/2 \end{cases} \qquad (3)$$

where and the angle of radiated power reaches maximum level at $\phi = 0$ and m_1 is Lambertian emission, it is expressed

$$m_1 = \frac{-\ln 2}{\ln(\cos\phi_{1/2})} \qquad (4)$$

where $\phi_{1/2}$ is LED semiangle at half-power,

The radiant intensity is expressed

$$s(\phi) = P_t \frac{(m_1+1)}{2\pi} \cos^{m_1}(\phi) \qquad (5)$$

where P_t is transmitted power. The intensity of the signal reaching the receiving system linearly at a certain angle from the light source in the illuminated environments is greater than the strength of the signals arriving by reflecting. LOS links enlarge the power effciency and reduce the multipath dispersion but short distance LOS has insignificant multipath dispersion that can be negligible. Channel impulse response (CIR) of LOS is given by

$$h_{los}(t) = \frac{A_r(m_1 + 1)}{2\pi d^2} \cos^{m_1}\phi T_s(\psi)g(\psi)\cos\psi\,\delta\left(t - \frac{d}{c}\right) \qquad (6)$$

where c is the speed of light, δ is delta dirac function, $\delta\left(t - \frac{d}{c}\right)$ presents the signal propagation delay. $T_s(\psi)$ is optical bandpass filter, $g(\psi)$ is a non-imaging concentrator of gain , d is a receiver location (check Fig. 7).

The average received power at the receiver is given

$$P_{r-los} = H_{los}(0)P_t \tag{7}$$

Where the channel gain $H_{los}(0)$, P_t is transmitted power. LOS optical link is given as

$$H_{los}(0) = \begin{cases} \dfrac{A_r(m_1 + 1)}{2\pi d^2} \cos^{m_1}\phi\, T_s(\psi)g(\psi)\cos\psi & 0 \le \psi_c \\ 0 & \text{elsewhere} \end{cases} \tag{8}$$

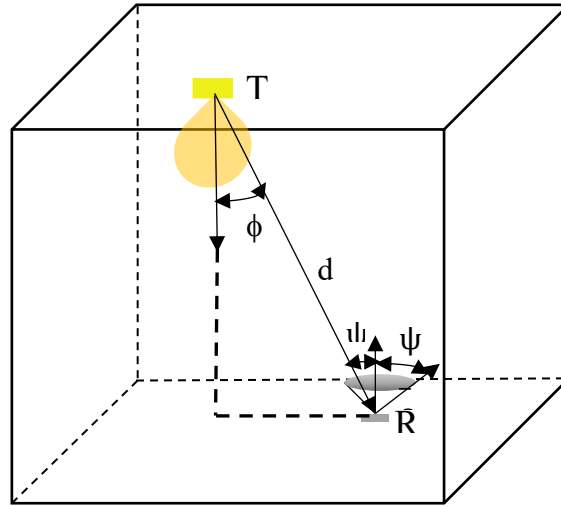
Fig. 7: LOS link model of the VLC [1].

1.2.2.   Non-line-of-sight (NLOS) VLC

NLOS communication systems are based on multipath propagation. NLOS happens in indoor enviromental systems and it is much more complex to predict than LOS links since NLOS optical link communicates with signals by reflection from walls, furnitures, people etc [34]. Morever, there are more factors that affects to

CIR such as wavelength, surface material, field of view (FOV), blockage and shadowing [35-37]. The collected signals by reflection causes energy loss on reflective surfaces. The average received power at photodetector is defined as [2]

$$P_r = P_t[H_{los}(0) + H_{nlos}(0)]$$
$$= P_t H_{los}(0) + P_t \sum_{refl} H_{refl}(0) \tag{9}$$

where $H_{refl}(0)$ is reflected path for DC gain and P_t is transmitted power and h_{nlos} is called channel impulse response in time domain that is expressed by

$$h_{nlos}(t, S, R_x) = \sum_{k=0}^{\infty} h_{nlos}^{(k)}(t, S, R_x) \tag{10}$$

where $h_{nlos}^{(k)}$ is the impulse response, k is the reflection numbers, S is single source and R_x is receiver.

If there is more than one source, K is multiple sources as a summation in the equation. It is given by

$$h_{nlos}(t, S, R_x) = \sum_{i}^{K} \sum_{k=0}^{\infty} h_{nlos\ K}^{(k)}(t, S, R_x) \tag{11}$$

After k reflection , the impulse response is expressed as

$$h_{nlos}(t, S, R_x) = \frac{(m_1+1)}{2\pi} \sum_{j=1}^{K} \rho_j \cos^{m_1}\left(\phi_j\right) \frac{\cos(\psi)}{d_{Sj}^2} rect\left(\frac{2\psi}{R}\right) \times h_{nlos}^{(k-1)}\left(t - \frac{d_{Sj}}{c}, E, R_x\right) \Delta A \tag{12}$$

where ΔA is the reflecting area, ρ_j reflection coefficient of E, d_{Sj} is distance between source and reflector E, $h_{nlos}^{(k-1)}$ is the CIR of k-1 order between j and R_x.

The channel impulse response is calculated by integrating the power as given (12). The root mean square delay spread (D_{rms}) is used for time distribution of multipath channel as given by [2]

$$D_{rms} = \left[\frac{\int(t-\mu)^2 h^2(t)dt}{\int h^2(t)dt}\right]^{\frac{1}{2}} \tag{13}$$

12

where the mean delay spread μ is espressed

$$\mu = \frac{\int th^2(t)dt}{\int h^2(t)dt} \tag{14}$$

If the D_{rms} is major , the CIR is more sensitive for frequency since the bandwidth decreases in the channel. If the D_{rms} decreases, frequency becomes proper in channel. In Fig. 8 shown channel impulse response for LOS and NLOS. The first reflection has a powerful signal in both LOS and NLOS. The multiple reflection of the signal from the light source retards arrival of the signal to the receiver, thereby, this causes to decrease the amplitude of the transmitted signal. As shown in Fig. 8 LOS channel impulse response has much more amplitude than NLOS channel impulse response. Besides, Number of peak of NLOS CIR increases by every reflection.
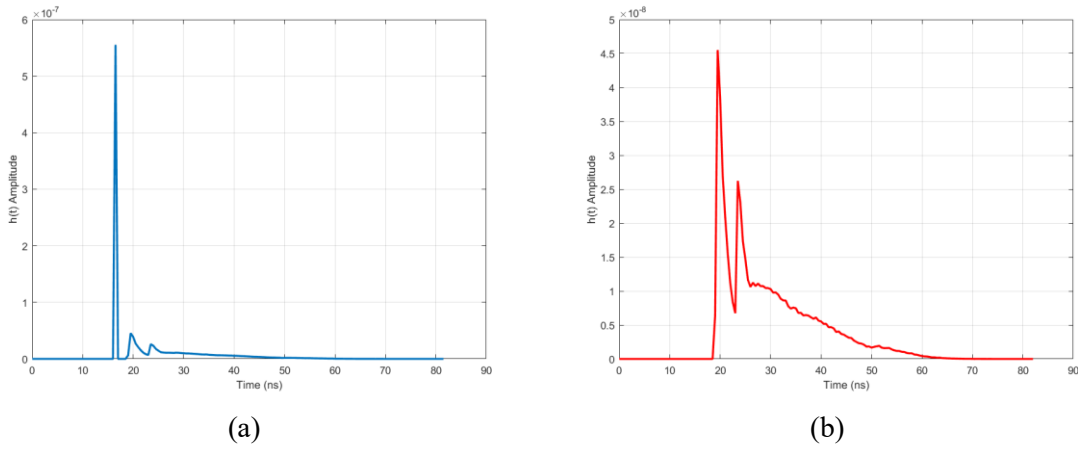

(a)   (b)

Fig. 8: Channel impulse responses (a) LOS and (b) NLOS [2].

1.2.3   Reflection Models

Reflection from any material is very significant for indoor NLOS VLC since receiver obtains not only directed light but also many scattered lights. In NLOS VLC, there are 3 types of reflection as shown in Fig. 9 depicted in [38].
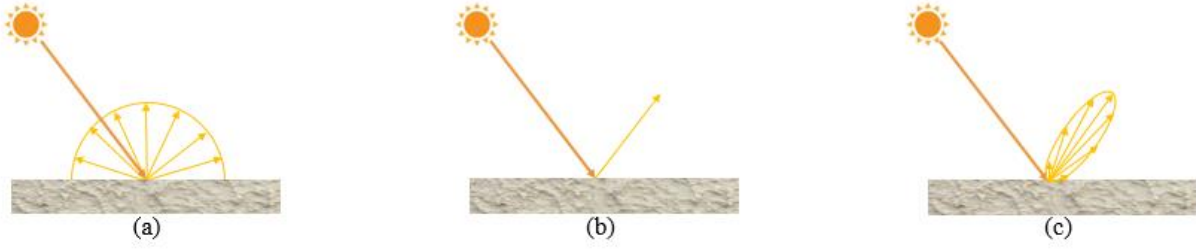
Fig. 9: Types of reflection. (a) diffuse reflection, (b) mirror/specular reflection and (c) glossy/specular reflection.

Mostly, diffuse (non-directed NLOS) reflection is observed by NLOS VLC in indoor enviroment. Light is reflected from a material.Concurrently, light scattering is observed and it is mainly called Lambert's model of reflection. Generally channel models are described by Monte Carlo ray tracing and Lambert reflection model.

The first order reflection is most significant in NLOS channel as the transmission paths are a significant factor in NLOS channel. Especially when the receiver is close to the edge of the room [2]. Some of models have been adopted from infrared communication systems [39]. There are two models commonly used to approximate the reflection: Lambert's model and Phong's model. Phong's model consists of Lambert's model which is called diffuse reflection is used for rugged surfaces.

As explained on wireless infrared communication in [40] has focused on two areas: the diffuse propagation and tracked directed link in indoor environments. The signal from transmitter is reflected off the walls of the room before reaching the receiver in NLOS channel. The signal travel around the room which could incident from any direction. Particularly, Monte Carlo Method/ray tracing is most useful to calculate channel impulse response (CIR) of the empty room in visible light wavelength [41,42].

Mirror/specular reflection, is also called perfectly specular reflectance, has only one path as shown in Fig. 9. The calculation requires only the reflection point. Then there is a single path through the receiver. It occurs on shiny materials such as metallic mirrors and it is defined [43],

$$L_{reflected}(\theta_r, \phi_r) = \rho_{sp} \cdot L_i(\theta_r, \phi_r \pm \pi) \tag{15}$$

For the ideal case ,

$$\rho_{sp}(\theta_i, \phi_i; 2\pi) = \lim_{K_r \to 0} \rho_{sp}(\theta_i, \phi_i; \theta_{0r} = \theta_i, \phi_{0r} = \phi_i \pm \pi, K_r) \tag{16}$$

Glossy/specular reflection is distributed ray tracing. Glossy reflection is expressed by bidirectional reflectance distribution functions (BRDFs).
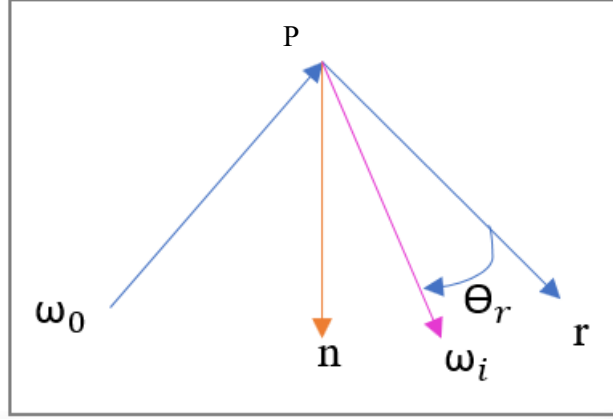
Fig. 10: Mirror and glossy reflection.

A ray hits on the surface from ω_0, where mirror reflection r , reflected way ω_i and it makes an angle θ_r between mirror reflection and reflected way.

The BRDF for the mirror reflection is shown [44],

$$f_{r,s}(p,\omega_i,\omega_0) = ck_r c_r \cos(\theta_r)^e = ck_r c_r (r\bullet\omega_i)^e \qquad (17)$$

where c is a normalization constant and e is specular exponent. It indicates that according as e increases, BRDF consistence increases around r.
The BRDF for the reflected radiance is shown [44],

$$L_{indirected}(p,\omega_0) = ck_r c_r \int\limits_{2\pi^+} (\omega_i \bullet r)^e L_0(r_c(p,\omega_i),-\omega_i)\cos\theta_i d\omega_i \qquad (18)$$

If the $\cos\theta_i$ is eliminated, where $\cos\theta_i = n\bullet\omega_i$ and the limit of $e\to\infty$, better glossy/specular reflection is obtained as shown,

$$p(\omega_{i,j})\infty(r\bullet\omega_i)^e(n\bullet\omega_i) \qquad (19)$$

15

1.2.4. Ray Tracing Methods

1.2.4.1. Monte Carlo Ray Tracing

The modified Monte Carlo ray tracing algorithm (MMCA) method ensures the estimation of the impulse response. It is used for calculation of diffuse optical channel by Lambertian (diffuse) or specular reflections [45]. If number of rays are enough to estimate the error, Monte Carlo simulation is necessary only once [46]. Probability density function (PDF) is used as a Lambertian pattern. The PDF executes the same optical power through the traced ray. However, Monte Carlo tracing ray from reflected point to receiver is taken into account to line-of-side (LOS) calculation and LOS impulse response is shown by [46],

$$P_R = \frac{1}{d^2} R_E(\phi, n) A_{eff}(\varphi) \tag{20}$$

where P_R received power, E emitter, R receiver, large distance between emitter and receiver d, Lambertian pattern. Besides, effective signal $A_{eff}(\varphi)$ shown as,

$$A_{eff}(\varphi) = A_r \cos\varphi \, rect\left(\frac{\varphi}{FOV}\right) \tag{21}$$

$$rect(x) = \begin{cases} 1, & |x| \leq 1 \\ 0, & |x| > 1 \end{cases} \tag{22}$$

And $R_E(\phi, n)$ is shown,

$$R_E(\phi, n) = \frac{n+1}{2\pi} P_E \cos^n(\phi), \qquad -\frac{\pi}{2} \leq \phi \leq \frac{\pi}{2} \tag{23}$$

where n is mode number of radiation lobe. Besides, it represents the direction of the transmitter. P_E is the radiated power of emitter. Lastly, A_r and FOV are the physical area of the receiver and the field of view of the receiver respectively.

1.2.4.2. Lambert's Model

Lambert's model is observed on smooth surfaces. Those surfaces reflect the light equally. The reflection patterns are precisely diffuse which are described as

$$R(\theta_0) = \rho R_i \frac{1}{\pi} \cos(\theta_0) \tag{24}$$

Where ρ is the reflection coefficient, R_i is the incident optical power and θ_0 is the observation angle. The important factor is that incidance angle does not play a role on the shape of the reflection pattern. Fig. 10 indicates Lambertian model. The bold lines represent the incidence direction and thin lines represent the direction of specular reflection.

Lambert's cosine law is using for emission from a LED [47].

$$m = -\frac{\ln(2)}{\ln(\cos(\vartheta_{1/2}))} \tag{25}$$

Where, m is the Lambertian radiant order and $\vartheta_{1/2}$ is transmitter semi-angle (at half power).

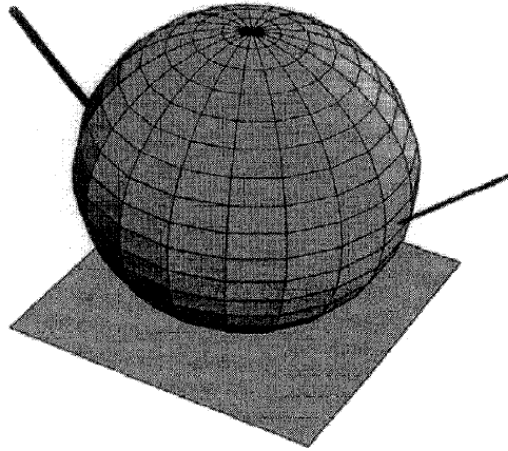Fig. 11: Reflection pattern of Lambert's model is depicted [39].

1.2.4.3. Phong's Model

Phong's model is more complex than Lambert's model. Despite it is not able to approach pattern, Phong's model evolved out of Lambert's model. Specular and diffuse reflections are observed by reflection pattern of rough surfaces. Those reflections are well approximated by Lambert's model. Phong's model described by

$$R(\theta_i, \theta_0) = \rho \frac{R_i}{\pi} \left\{ r_d \cos(\theta_0) + (1 - r_d) \cos^m(\theta_0 - \theta_i) \right\}$$

(26)

Where r_d is percentage of incident signal, θ_i is incident angle and the parameter m controls the directivity of the specular component of the reflection.
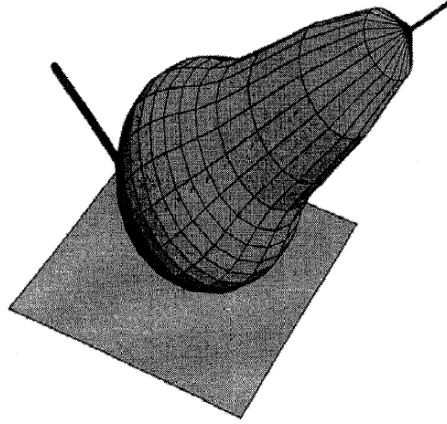

Fig. 12: Phong's model reflection pattern depicted [39].

1.2.4.4. Recursive Method

Using recursive method the impulse response after k reflection is calculated as in equation (11)

$$h(t, S, R_x) = \frac{m_1 + 1}{2\pi} \sum_{j=1}^{K} \rho_j \cos^{m_1}(f_j) \frac{\cos(\psi)}{d_{Sj}^2} \text{rect}\left(\frac{2\psi}{\pi}\right) x h_{nlos}^{k-1}\left(t - \frac{d_{Sj}}{c}, E, R_x\right) \Delta A$$

(27)

where ρ_j is the reflection coefficient of E, ΔA is the area of LED,K is the total number of reflector elements, ρ_j is reflection coefficient of j, d_{Sj} is the distance from S transmitter to $E, h_{nlos}^{k-1}\left(t - \frac{d_{Sj}}{c}, E, R_x\right) \Delta A$ is impulse response of order k-1 between reflector and R_x.

Recursive least square (RLS) algorithm is an equalization method that which the coefficients are iteratively determined. It provides very fast convergence.
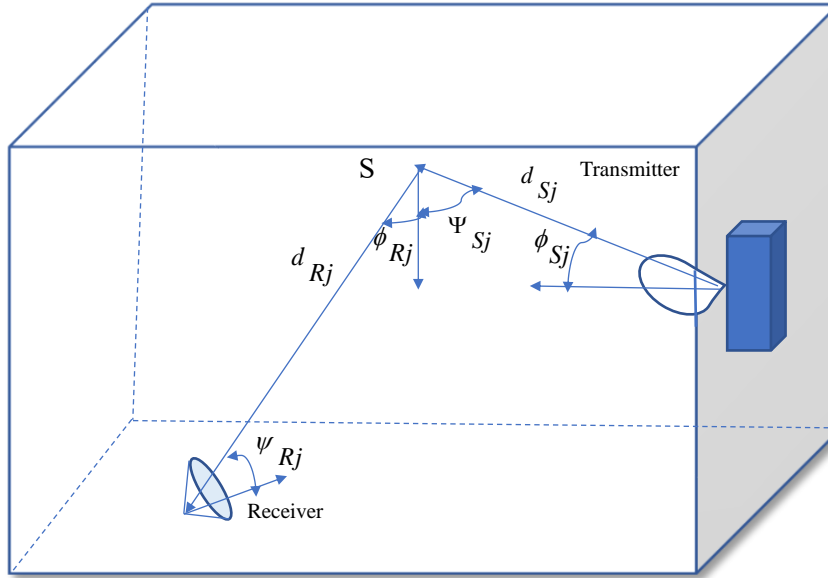
Fig. 13: The geometry of NLOS impulse response by recursive method.

2. RESULTS

2.1. Measurement

The measurement part has been completed in the optical laboratory at Czech Technical University. The diploma thesis has focused on experimentally analyse utilization of NLOS VLC to derive optical channel impulse responses using ray-tracing model. Besides it has analysed experimentally BER performance in case of VLC link with reflection from different distances and degrees.

Components of the measurement are DC power supply, driver, White LED, lenses, white paper, photodetector, oscilloscope, signal generator and laptop for observing the results.
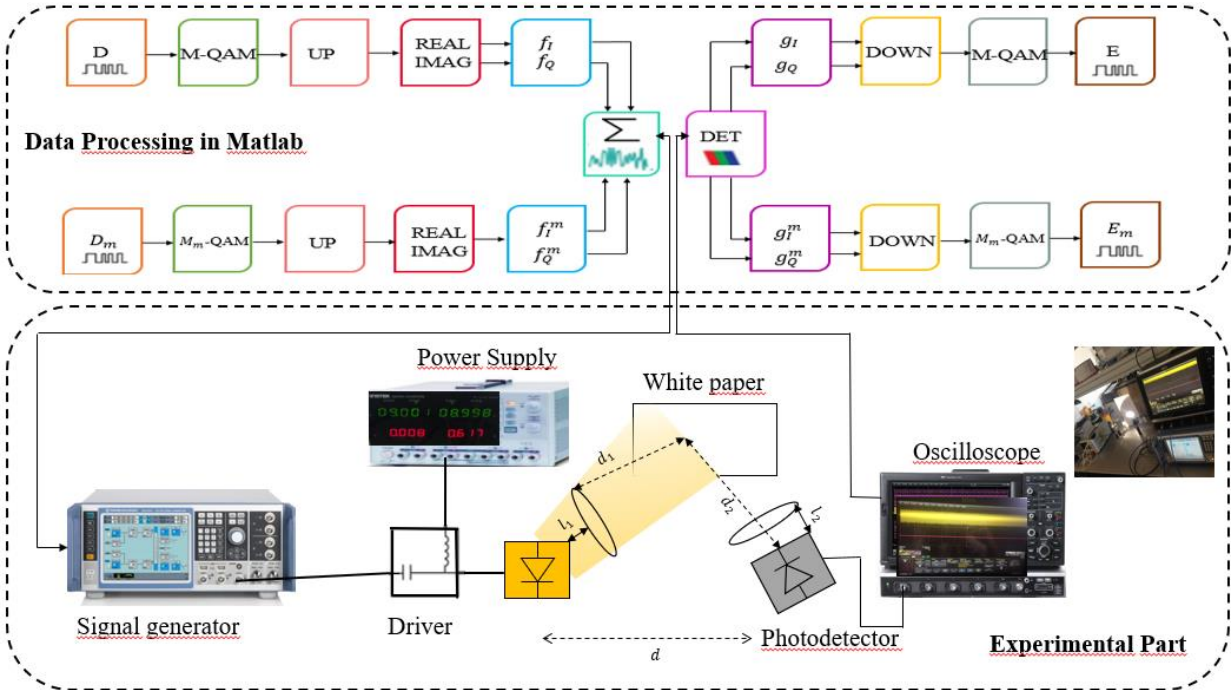
Fig. 14: m-CAP block diagram [30].

As shown in Fig. 14, upper part is data processing in Matlab, bottom part is experimental part in laboratory environment. D is input streams, DET is determined signal , g is matched filtering and E is estimated received bits [32,48].

As shown in Fig. 14 and Fig.15, firstly, vector signal generator generates the QAM signal using m-CAP (10-CAP) modulation which is in 1 MHz frequency and 11.98 dBm (0.0158 W) peak envelope power. LED driver converts the input voltage to optimal utilizable voltage for LED before input data is generated. Then, the lens collimates the light due to the light scattering. The diffuse reflection occurs on the white paper. It is also called Lambert's model. After that, scattered lights goes through the photo-detector as the collimated lens collects the scattered lights to the photo-detector. Finally, the result is observed by the oscilloscope.
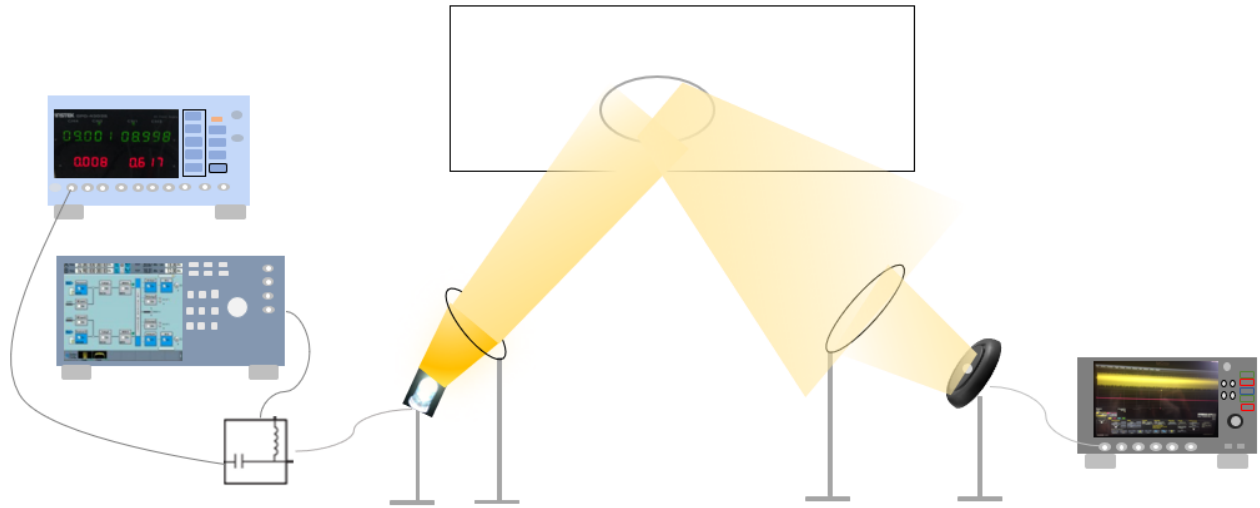
Fig. 15: Scheme of measurement.

TABLE 3. Components of measurement.

DC power supply ⟶	Instek GPD-430S DC: 9V / 590 mA
Driver ⟶	Bias tee
White LED ⟶	Osram Golden Dragon
Lens ⟶	Focal length is 25 mm and 35 mm for transmitter and receiver, respectively.
Photodetector ⟶	PDA10A
Oscilloscope ⟶	LeCroy 640Zi
Signal generator ⟶	R&S SMW200A
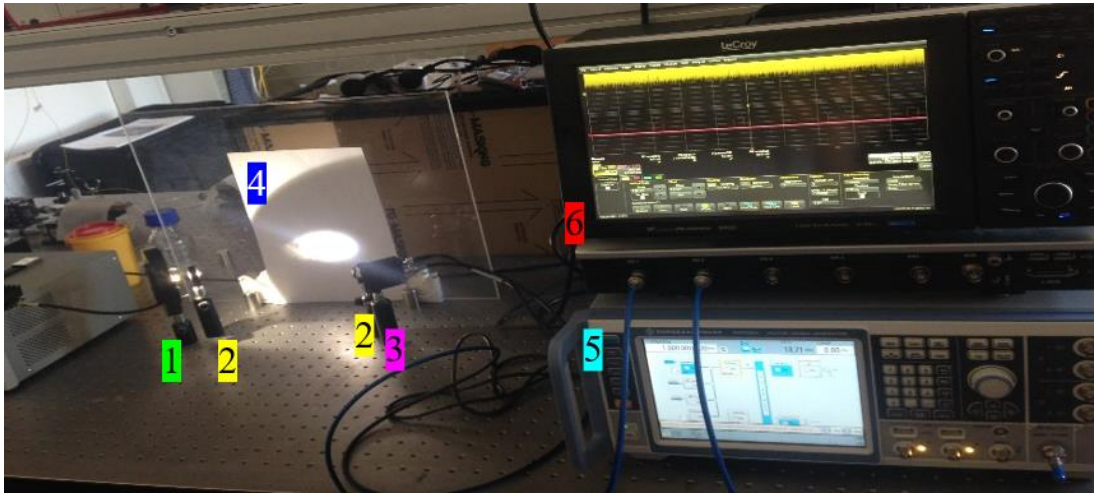
Fig. 16: Experimental part of the master diploma thesis.

As shown in the both pictures Fig. 16 and Fig. 17, 1.White LED , 2.Lens, 3.Photodetector, 4.White Paper, 5.Signal generator, 6. Oscilloscope.
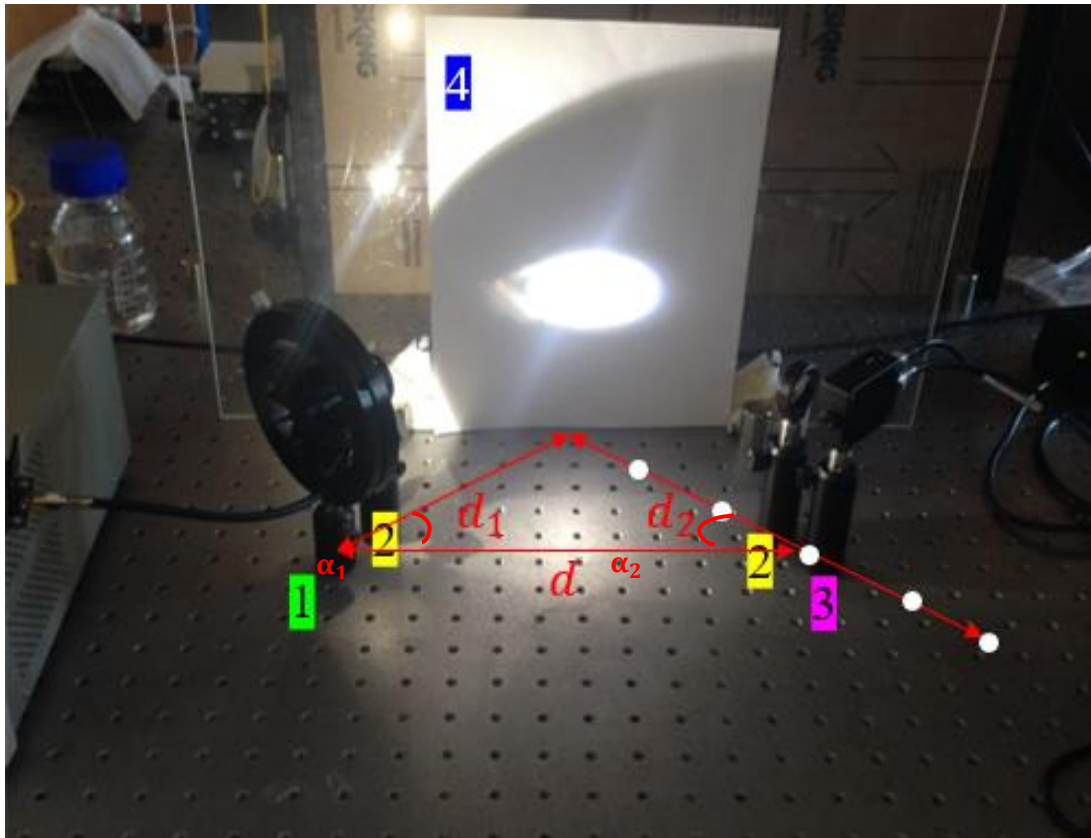
Fig. 17: Frontal view of experimental part of the master diploma thesis.

As shown as the red highlight d, d_1 and d_2 are distance of between transmitter- receiver, transmitter and receiver respectively. α_1 and α_2 are degree of transmitter and receiver.

Fig. 18: BER performance on the white paper, transmitter (TX) 20cm, receiver (RX) distance from 10 to 50 cm, angle of trasmitter 30° and k=1bit.

As shown in Fig. 18, W10-50=W10: White paper, RX=10 cm and TX=50 cm. W20-50=W20: White paper, RX=20 cm and TX=50 cm, W30-50=W30: White paper, RX=30 cm and TX=50 cm, W40-50=W40: White paper, RX=40 cm and TX=50 cm, W50-50=W50: White paper, RX=50 cm and TX=50 cm. The transmitter is at 50 cm. Bit error rate is higher at receiver 50 cm and smaller at receiver 10 cm as we expected where the transmitter and receiver have 30 degree.
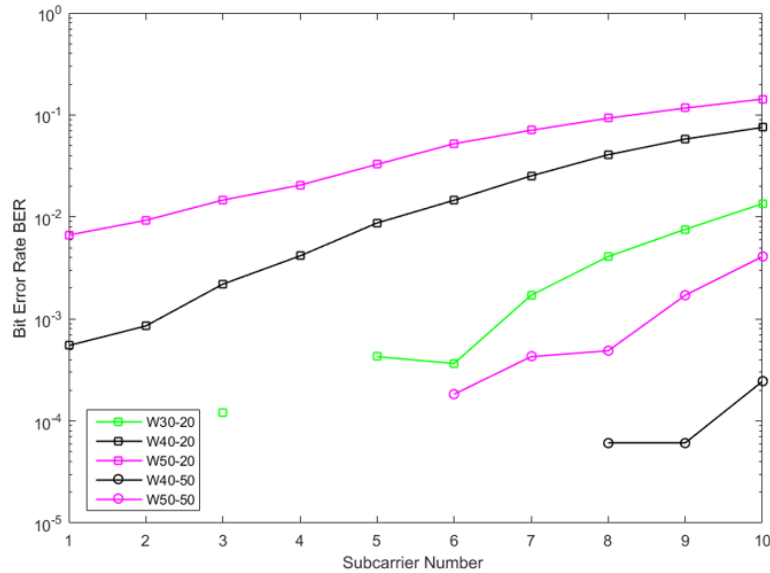
Fig. 19: BER performance on the white paper, transmitter (TX) 20 cm and 50 cm, receiver (RX) distance from 30 to 50 cm, angle of trasmitter 45° and k=1bit.

As shown in Fig. 19, W30-20=W30: White paper, RX=30 cm and TX=20 cm, W40-20=W40: White paper, RX=40 cm and TX=20 cm, W50-20=W50: White paper, RX=50 cm and TX=20 cm, W40-50=W40: White paper, RX=40 cm and TX=50 cm, W50-50=W50: White paper, RX=50 cm and TX=50 cm. The graph indicates that bit error rate is higher at transmitter 20 cm. BER is higher when the receiver at 50 cm in both case where the transmitter and receiver have 45° angle.
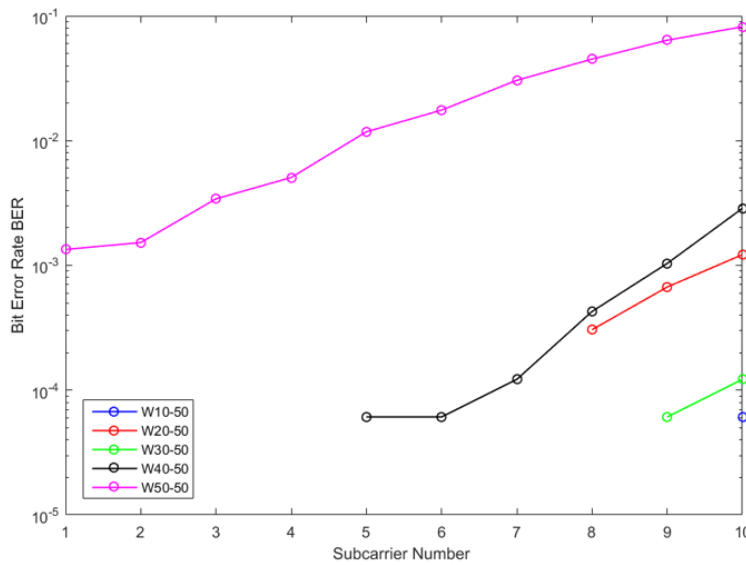
Fig. 20: BER performance on the white paper, transmitter (TX) is 20 cm, receiver (RX) distance is from 30 to 50 cm, angle of trasmitter is 45° and k is 1bit.

As shown in Fig. 20, W30=W30: White paper, RX=30 cm, W40=W40: White paper, RX=40 cm, W50=W50: White paper, RX=50 cm. The transmitter is at 20 cm. Bit error rate is higher at receiver 50 cm and smaller at receiver 30 cm as we expected where the transmitter and receiver have 45 degree.

Fig. 21: BER performance on the white paper, transmitter (TX) is 20 cm, receiver (RX) distance is from 30 to 50 cm, angle of trasmitter is 60° and k is 1bit.

As shown in Fig. 21, W30=W30: White paper, RX=30 cm, W40=W40: White paper, RX=40 cm, W50=W50: White paper, RX=50 cm. The transmitter is at 20 cm. Bit error rate is higher at receiver 50 cm and smaller at receiver 30 cm, as we expected where the transmitter and receiver have 60° angle.


Fig. 22: BER performance on the black cotton material, transmitter (TX) 20cm, receiver (RX) distance from 10 to 50 cm, angle of trasmitter 60° and k=1bit.

As shown in Fig. 22, B10-60=B10: Black cotton material, RX=10 cm and TX=60°. B20-60=B20: Black cotton material, RX=20 cm and TX=60°, B30-60=B30: Black cotton material, RX=30 cm and TX=60°, B40-60=B40: Black cotton material, RX=40 cm and TX=60°, B50-60=B50: Black cotton material, RX=50 cm and TX=60°. BER of the black material is very high.
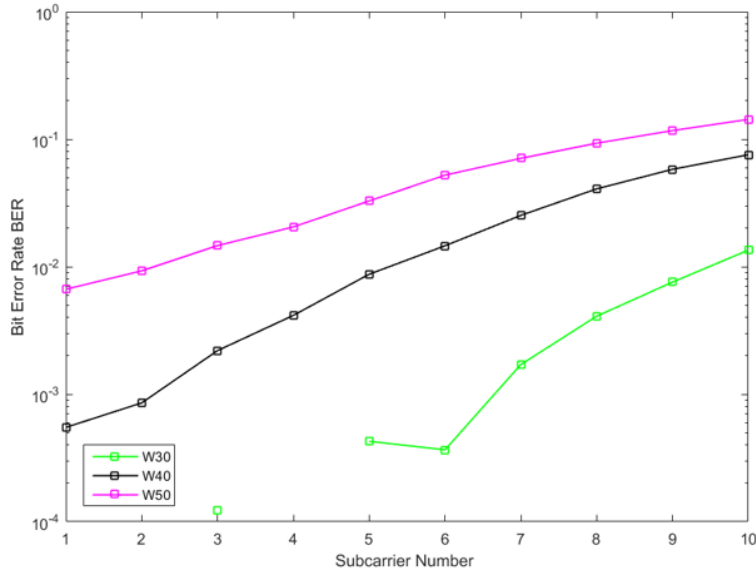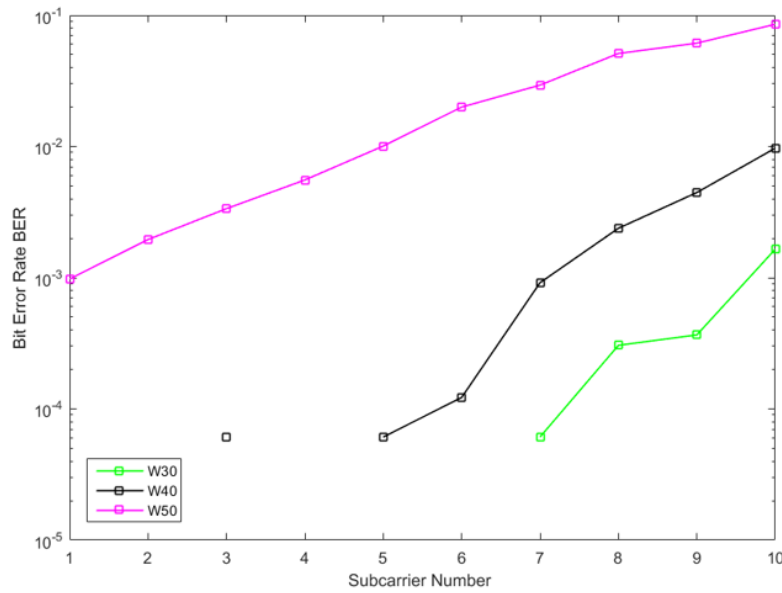
Fig. 23: BER performance on the white paper, transmitter (TX) is 20 cm, receiver (RX) distance is from 30 to 50 cm, angle of trasmitter is 75° and k is 1bit.

As shown in Fig. 23, W30=W30: White paper, RX=30 cm, W40=W40: White paper, RX=40 cm, W50=W50: White paper, RX=50 cm. The transmitter is at 20 cm. Bit error rate is higher at RX 50 cm and smaller at RX 30 cm where TX has 75° angle.

Fig. 24: Comparison BER performance on the black cotton material and on the white paper, transmitter (TX) 20cm, receiver (RX) distance from 10 to 50 cm, angle of trasmitter 30° and k=2bits.

As shown in Fig. 24, B10-30-2=B10: Black cotton material, RX=10 cm, TX=30° and k=2bits, B20-30-2=B20: Black cotton material, RX=20 cm, TX=30° and k=2bits, B30-30-2=B30: Black cotton material, RX=30 cm, TX=30° and k=2bits, B40-30-2=B40: Black cotton material, RX=40 cm, TX=30° and k=2bits, B50-30-2=B50: Black cotton material, RX=50 cm, TX=30° and k=2bits. The transmitter is at 20 cm. For black cotton material, Bit error rate is higher at RX 50 cm and smaller at RX 10 cm. Moreover, on the white paper, BER is lower than BER of black cotton material.
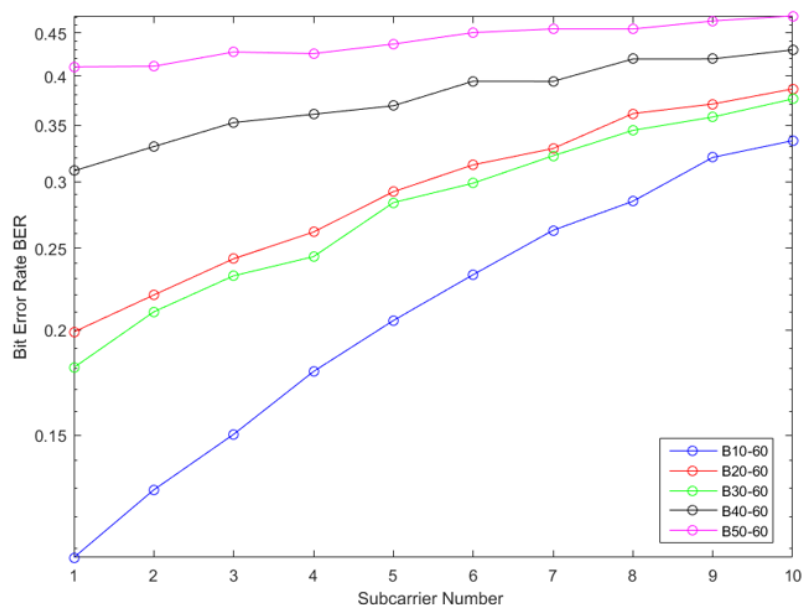
Fig. 25: BER performance on the white paper, transmitter (TX) 20 cm, receiver (RX) distance from 10 to 50 cm, angle of trasmitter 45° and k=4bits.

As shown in Fig. 25, W10-45-4=W10: White paper, RX=10 cm, TX=45 ° and k=4bits,W20-45-4=W20:White paper, RX=20 cm, TX=45° and k=4bits, W30-45-4=W30: White paper, RX=30 cm TX=45° and k=4bits, W40-45-4=W40: White paper, RX=40 cm, TX=45° and k=4bits, W50-45-4=W50:White paper, RX=50 cm TX=45° and k=4bits. Transmitter is at 20 cm and its angle is 45° for 4 bits. BER is highest performance at the RX 50 cm and lowest performance is at 10 cm.
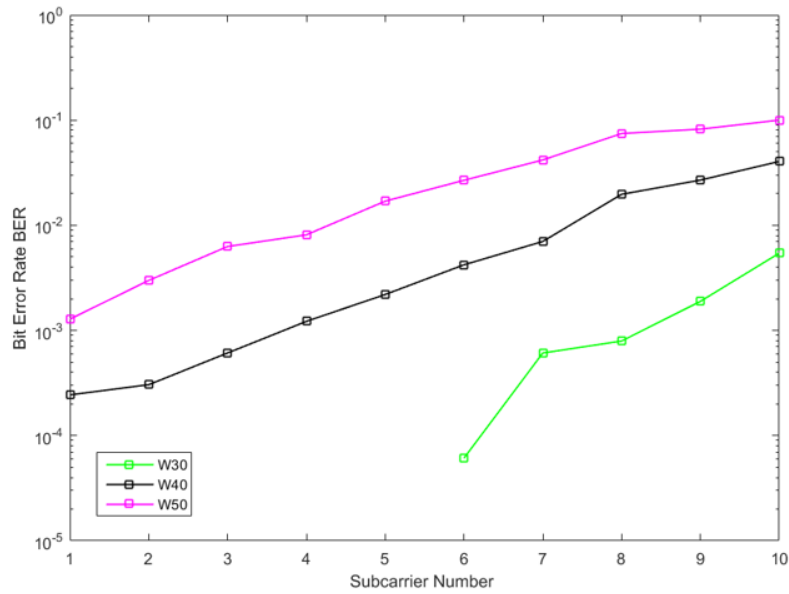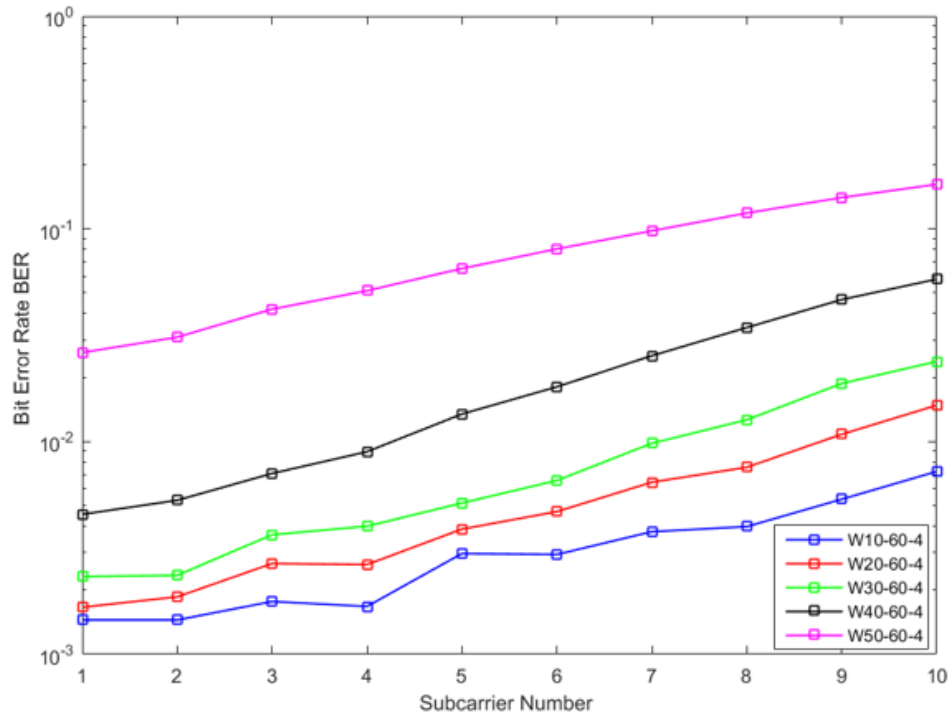
Fig. 26: BER performance on the white paper, transmitter (TX) 20 cm, receiver (RX) distance from 10 to 50 cm, angle of trasmitter 60° and k=4bits.

As shown in Fig. 26, W10-60-4=W10:White paper, RX=10 cm, TX=60° and k=4bits,W20-60-4=W20:White paper, RX=20 cm, TX=60° and k=4bits, W30-60-4=W30: White paper, RX=30 cm TX=60° and k=4bits, W40-60-4=W40: White paper, RX=40 cm, TX=60° and k=4bits, W50-60-4=W50:White paper, RX=50 cm TX=60° and k=4bits. Transmitter is at 20 cm and its angle is 60° for 4 bits. the transmitter is at 20 cm. As I expected, bit error rate is higher at receiver 50 cm and smaller at receiver 10 cm.
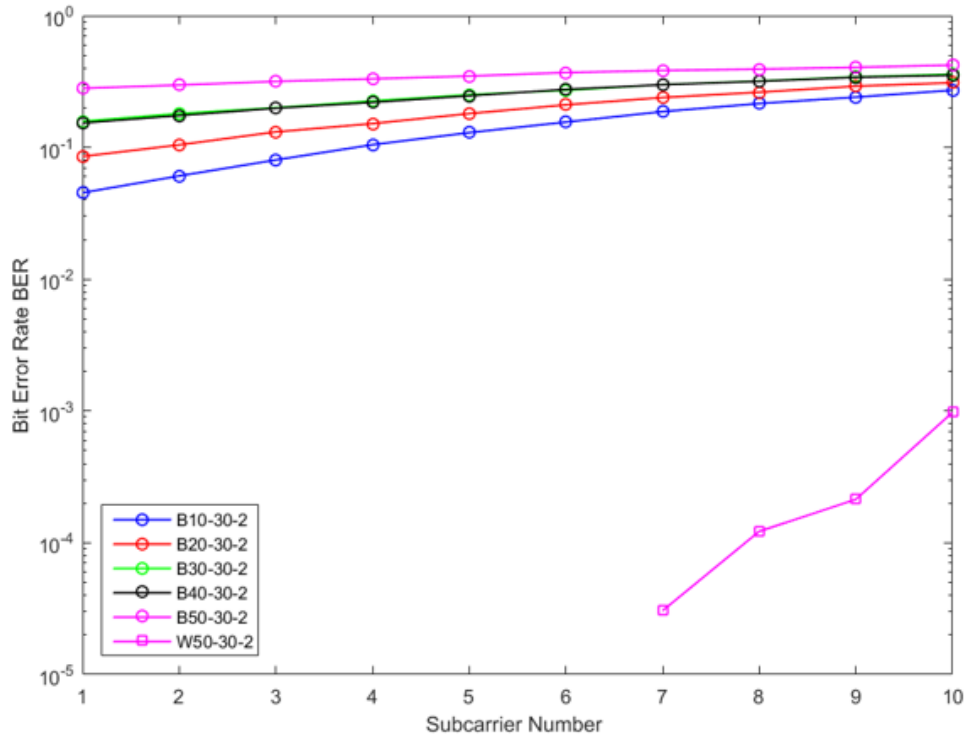
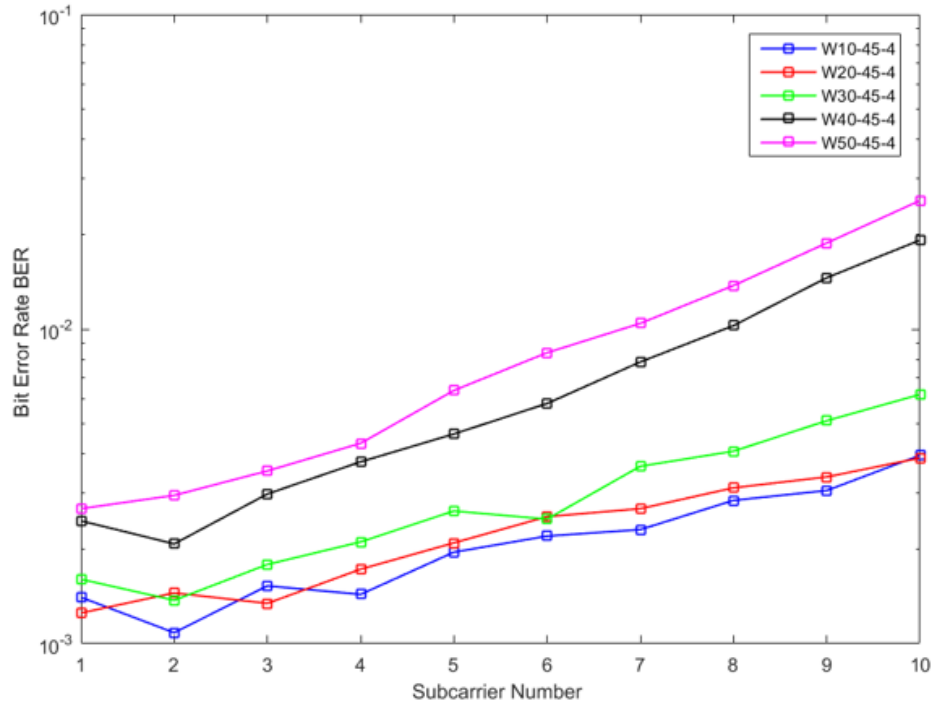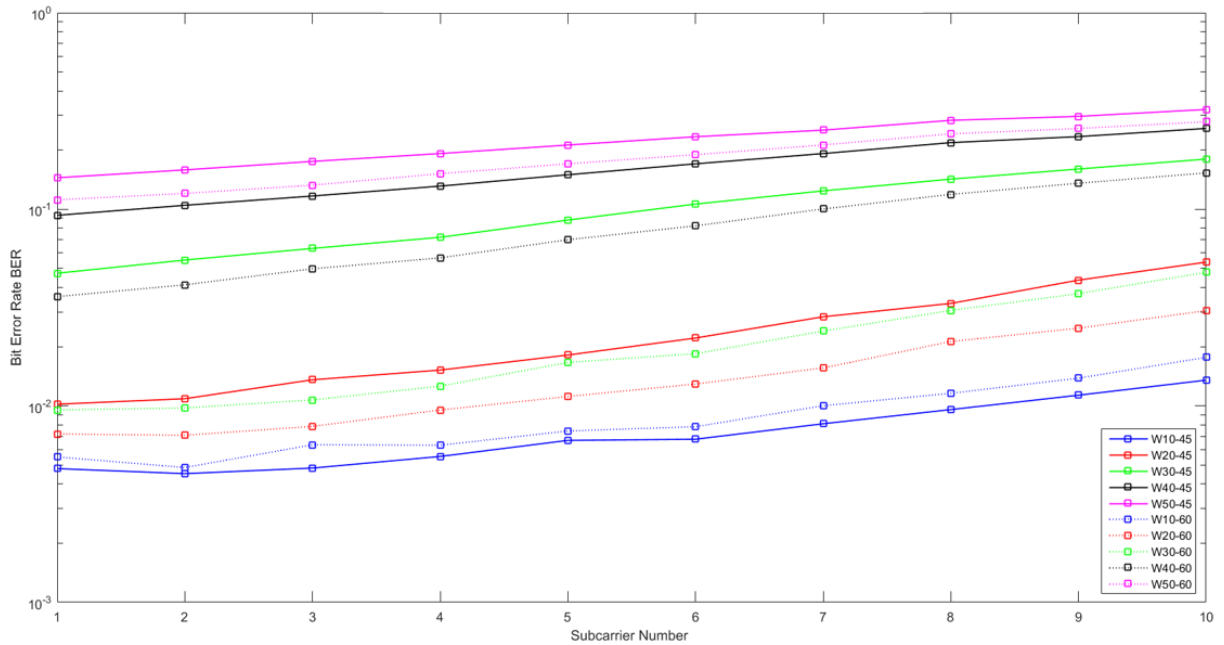Fig. 27: Comparison BER performance on the white paper, transmitter (TX) 20cm, receiver (RX) distance from 10 to 50 cm, angle of trasmitter 45° and 60°, k=4bits.

As shown in Fig. 27, W10-45=W10: White paper, RX=10 cm and TX=45°. W20-45=W20: White paper, RX=20 cm and TX=45°, W30-45=W30: White paper, RX=30 cm and TX=45°, W40-45=W40: White paper, RX=40 cm and TX=45°, W50-45=W50: White paper, RX=50 cm and TX=45°. W10-60=W10: White paper, RX=10 cm and TX=60°. W20-60=W20: White paper, RX=20 cm and TX=60°, W30-60=W30: White paper, RX=30 cm and TX=60°, W40-60=W40: White paper, RX=40 cm and TX=60°, W50-60=W50: White paper, RX=50 cm and TX=60°. 45° angle of transmitter has higher BER performance than 60° angle of transmitter.
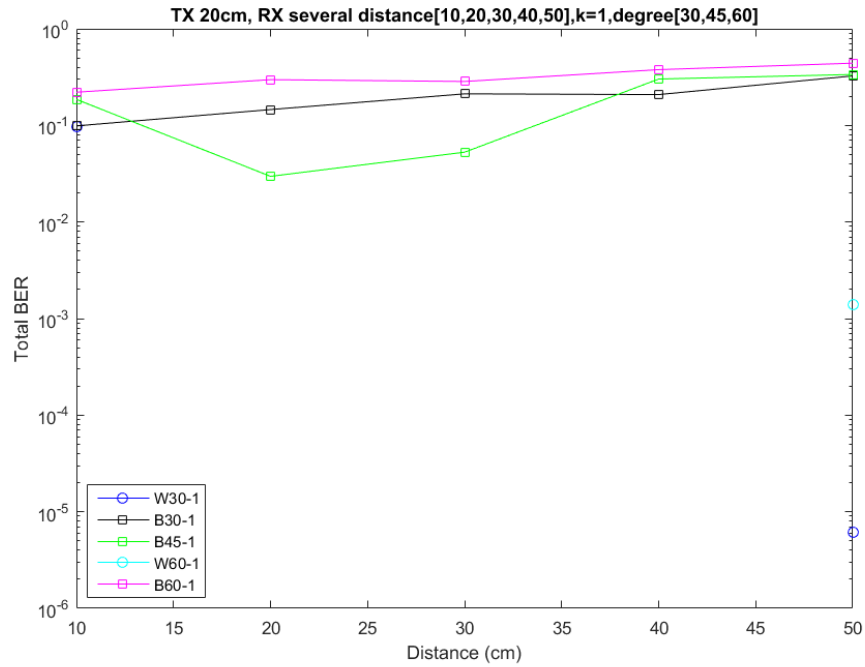
Fig. 28: Comparison of reflection on the white paper and black cotton material, transmitter (TX) 20cm, receiver (RX) distance from 10 to 50 cm, angle of trasmitter 30°, 45° and 60° , k=1bit.

As shown in Fig. 28, W30-1=W30: White paper, TX=30° and k=1bit, B30-1=B30: Black cotton material, TX=30° and k=1bit, B45-1= Black cotton material, TX=45° and k=1bit, W60-1= White paper, TX=60° and k=1bit, B60-1= Black cotton material, TX=60° and k=1bit.

Fig.28 shows BER performance comparison with different angle of transmitter and receiver at 30° ,45° and 60°. As shown in the figure, both material has a highest BER at 50 cm receiver. When the transmitter is in 30° and 60°. BER on the white paper is higher when the transmitter is in 60° position than in 30° position. As I expected, black metarial has always highest BER performance than white paper. Black color absorbs all the visible lights and reflects almost none of them. White color reflects all the visible lights and absorbs almost none of them.

2.2. Simulations

In this chapter, I indicated modelling of the reflection of infrared signals in indoor environment. Some works [49-51] indicated the diffuse reflection and channel impulse response in various indoor environments. In [52] worked on recursive method to find third order reflection in an empty room. They observed that when the transmitter located at the center of the ceiling and the receiver looking ceiling located at the corner of the floor, impulse response $1.09x10^{-6}$. With the same transmitter the receiver with 45 degrees rotation located at the corner, impulse response is $1.35x10^{-6}$ so, it increases. In simulation part of the diploma thesis, I showed the transmitter located on the right side of the wall and the receiver location is changing with 30

degrees due to the simulation. I found out that how to obtain normalization of impulse reponse by using curve fitting on the simulation. Moreover, I observed how impulse response changes due to user orientation in time and frequency domain in different position of the room. The result shows that Phong's model is very complex than Lambert's model. Despite it is not able to approach pattern, Phong's model evolved out of Lambert's model. Lambert's model is for smooth surfaces which are totally irregular and reflect IR signals.
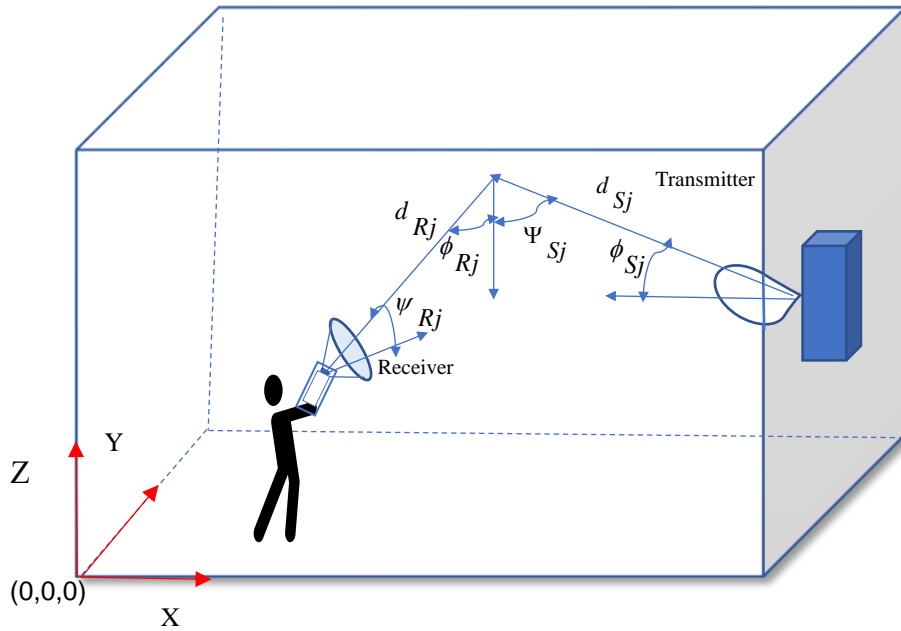
Fig. 29: The geometry of simulation part of the thesis.

Fig. 29 indicates the rectangular empty room shape in X,Y,Z coordination which is 5x5x3 m^3 as shown in Table 4. I assumed that there is a cell phone user in the room. He was holding his phone with 5° and 30° elevation angle respectively. For both angles, the user was turning around himself. During this period for both elevation angle, I have taken the results when user was at 90°,45°, 0°, -45° and -90° azimuth angle. I took into account that for the all the walls inside the room have the same reflection coefficient which is 0.73. The receiver is on the wall in front of the transmitter and its active area was 1 cm^2. Half angle FOV was 70°. 1W was considered for the power.

TABLE 4

PARAMETERS FOR THE SIMULATION

PARAMETER	VALUE
Room size	5x5x3 m^3
$\rho_{north,south,west,east,floor,ceiling}$	0.73
Source Location (x,y,z)	(5,2.5,1.5)
Source Elevation	180°
Source Azimuth	0°
Power	1 W
Receiver Location (x,y,z)	(1.6,1.8,1.5)
Receiver Elevation	5°,30°
Receiver Azimuth	[-90,90]
Active Receiver Area	1 cm²
Δt	0.5 ns
Half-angle FOV	70°
k (number of reflections)	3
Responsivity of detector	0.53
N (number of generated rays)	100000

Table 1. Simulation parameters.

 The simulation part impulse response demonstrates the intensity of the light. In other words, how much deeply possible to get data transmission. The whole frequency response calculated by the Fourier transform of the impulse response of the main reflections. Non-line-of-sight diffuse link modified by Monte Carlo Ray Tracing Method. For example, when receiver is in front of the transmitter, channel impulse response is lower than the other orientations due to scattering from wall.

The equation of normalization of the impulse response in time domain was shown in (28).

$$P(t)=P_{max}(t)e^{-nt} \tag{28}$$

Where , P is curve fitting of power, P_{max} is maximum power, m is number of curve and t is the time.

Channel Impulse Response and Transmitter-Receiver Orientation and Simulation Results

(a)   (b)

n=8.0

Fig. 30: Non-line-of-sight diffuse reflections (a) channel impulse response in time domain, (b) channel magnitude response in frequency domain simulated result (blue curve), approximation (red curve) for 5° elevation angle of transmitter. (a) indicates reflection of infrared signals from 90° azimuth angle of transmitter. The highest peak is the most significant for indoor NLOS channel. For this case, the lowest performance of the impulse response was observed that is 0.35. The normalization of the impulse response is that m equals to 8.0. (b) indicates frequency response which has also lowest power ratio at the lowest frequency.

n=9.1

Fig. 31: Non-line-of-sight diffuse reflections (a) channel impulse response in time domain, (b) channel magnitude response in frequency domain simulated result (blue curve), approximation (red curve) for 5° elevation angle of transmitter. (a) indicates reflection of infrared signals from 45° azimuth angle of transmitter. For this case, first higher order reflection of impulse response is 0.58. The normalization of the impulse response that m equals to 9.1. (b) indicates the frequency response which is higher power ratio than 90° azimuth angle of transmitter at the lowest frequency.

(a)

(b)

n=10.0

Fig. 32: Non-line-of-sight diffuse reflections (a) channel impulse response in time domain, (b) channel magnitude response in frequency domain simulated result (blue curve), approximation (red curve) for 5° elevation angle of transmitter. (a) indicates reflection of infrared signals from 0° azimuth angle of transmitter. For this case, first higher order reflection of impulse response is 0.87. The normalization of the impulse response that m equals to 10.0. I observed better result for 0° azimuth angle due to orientation of the transmitter. Its position is in front of the receiver. After the reflections, it received more signal from the transmitter. (b) indicates that power ratio has the highest value at this position of the transmitter at the lowest frequency.
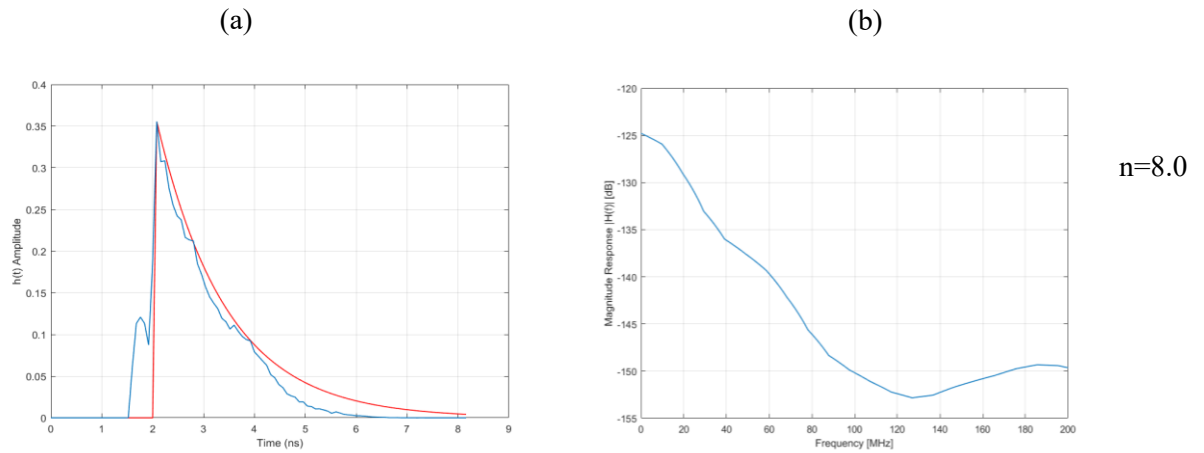
(a)   (b)

n=9.0

Fig. 34: Non-line-of-sight diffuse reflections (a) channel impulse response in time domain, (b) channel magnitude response in frequency domain simulated result (blue curve), approximation (red curve) for 5° elevation angle of transmitter. (a) indicates reflection of infrared signals from -45° azimuth angle of transmitter. For this case, first higher order reflection of impulse response is 0.45. The normalization of the impulse response that m equals to 9.0. (b) indicates the frequency response which is lower power ratio than 45° azimuth angle at the lowest frequency.
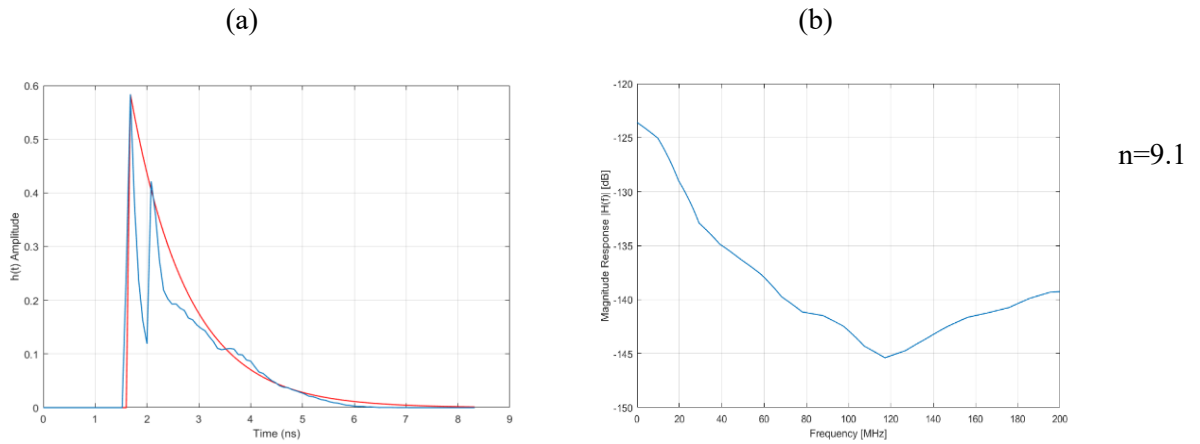
(a)   (b)

n=8.4

Fig. 35: Non-line-of-sight diffuse reflections (a) channel impulse response in time domain, (b) channel magnitude response in frequency domain simulated result (blue curve), approximation (red curve) for 5° elevation angle of transmitter. (a) indicates reflection of infrared signals from -90° azimuth angle of transmitter. For this case, first higher order reflection of impulse response is 0.4. The normalization of the impulse response that m equals to 8.4. (b) indicates the frequency response which is lower power ratio than 90° azimuth angle at the lowest frequency.
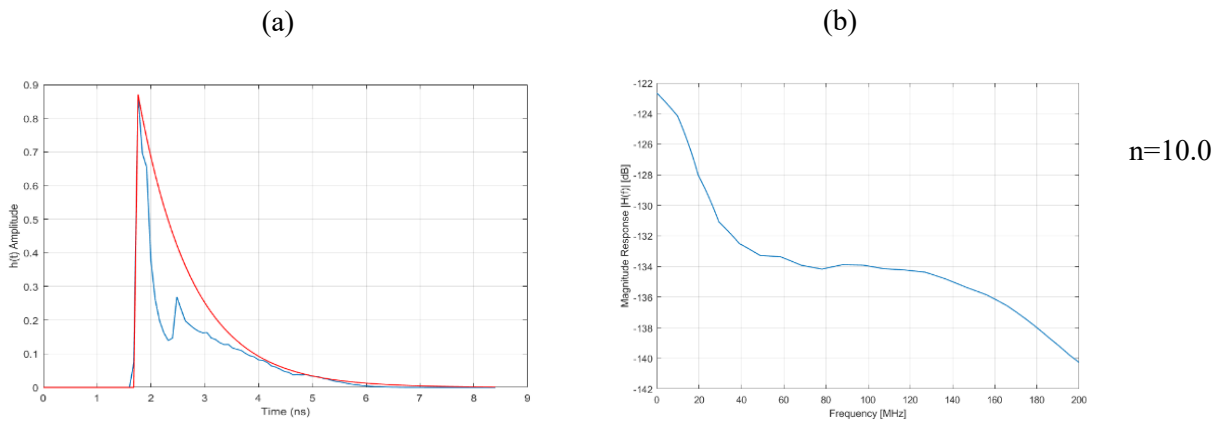
(a)   (b)

n=8.0

Fig. 36: Non-line-of-sight diffuse reflections (a) channel impulse response in time domain, (b) channel magnitude response in frequency domain simulated result (blue curve), approximation (red curve) for 30° elevation angle of transmitter. (a) indicates reflection of infrared signals from 90 ° azimuth angle of transmitter. The highest peak is the most significant for indoor NLOS channel. The impulse response was observed that is 0.35. The normalization of the impulse response is that m equals to 8.0. (b) indicates frequency response which has lowest power ratio at the lowest frequency same as -90° azimuth angle of transmitter.
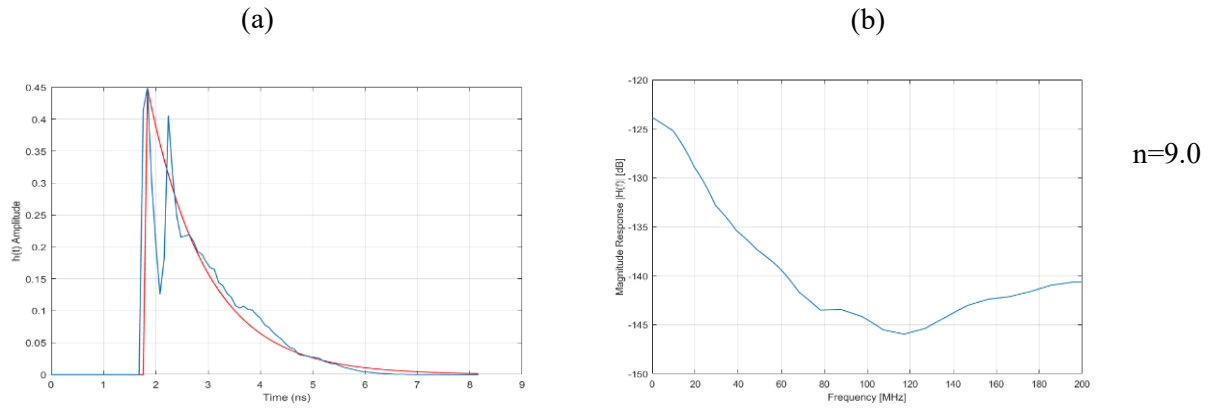
(a)   (b)

n=9.0

Fig. 37: Non-line-of-sight diffuse reflections (a) channel impulse response in time domain, (b) channel magnitude response in frequency domain simulated result (blue curve), approximation (red curve) for 30° elevation angle of transmitter. (a) indicates reflection of infrared signals from 45 ° azimuth angle of transmitter. For this case, first higher order reflection of impulse response is 0.54. The normalization of the impulse response that m equals to 9.0. (b) indicates the frequency response which is same power ratio as -45 ° azimuth angle of transmitter at the lowest frequency.

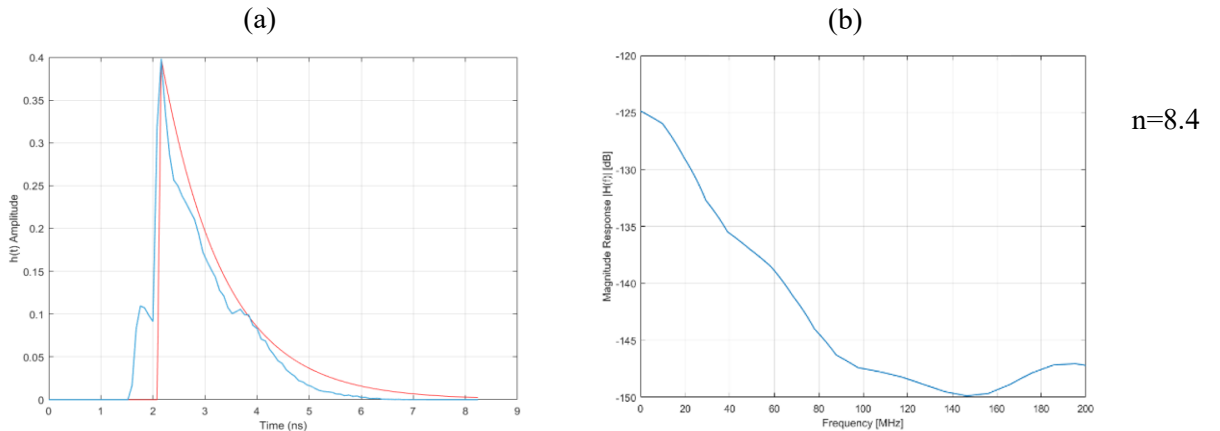(a)   (b)

n=10
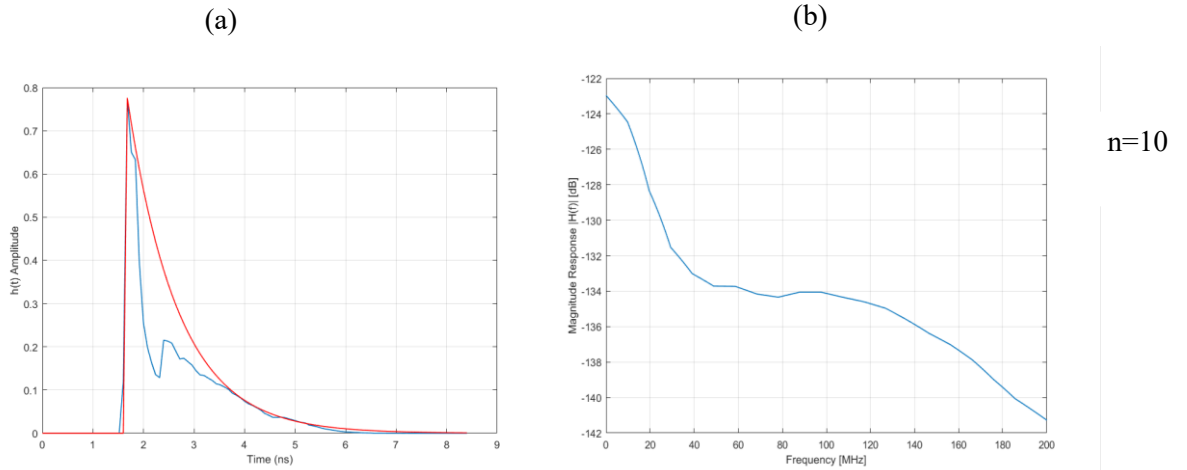
Fig. 38: Non-line-of-sight diffuse reflections (a) channel impulse response in time domain, (b) channel magnitude response in frequency domain simulated result (blue curve), approximation (red curve) for 30° elevation angle of transmitter. (a) indicates reflection of infrared signals from 0° azimuth angle of transmitter. For this case, first higher order reflection of impulse response is 0.82. The normalization of the impulse response that m equals to 10.0. I observed better result for 0° azimuth angle due to orientation of the transmitter. Its position is in front of the receiver. After the reflections, it received more signal from the transmitter. (b) indicates that power ratio has the highest value at the lowest frequency of this position.

(a)   (b)
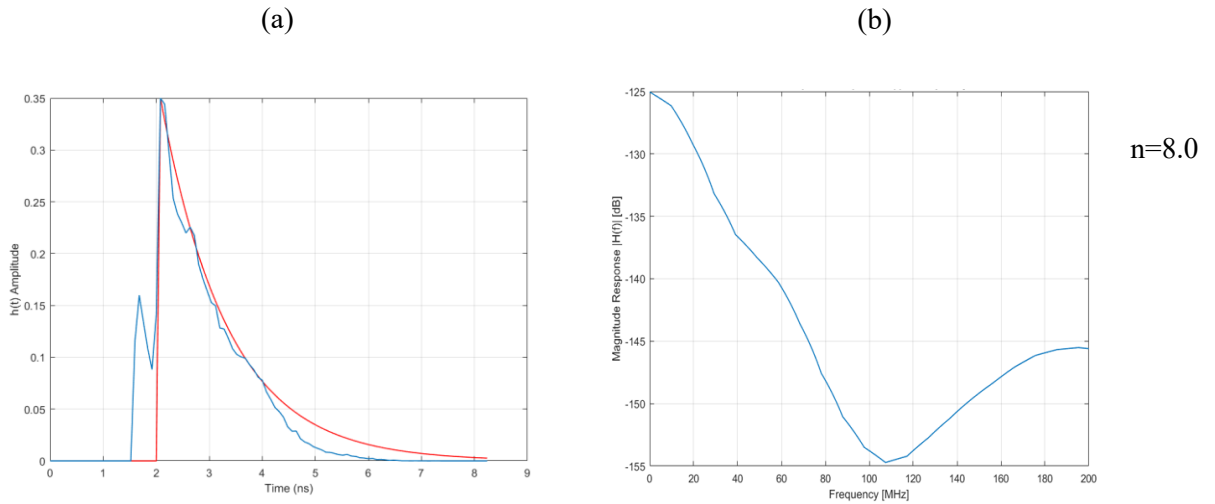
n=9.0
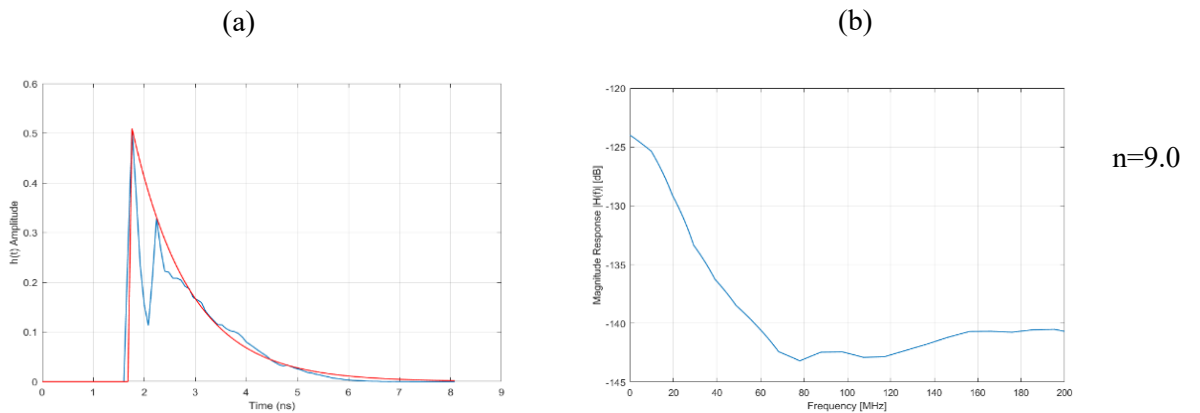
Fig. 39: Non-line-of-sight diffuse reflections (a) channel impulse response in time domain, (b) channel magnitude response in frequency domain simulated result (blue curve), approximation (red curve) for 30° elevation angle of transmitter. (a) indicates reflection of infrared signals from -45° azimuth angle of transmitter. For this case, first higher order reflection of impulse response is 0.51. The normalization of the impulse response that m equals to 9.0. (b) indicates the frequency response which is same power ratio than 45° azimuth angle as mentioned on the (a).

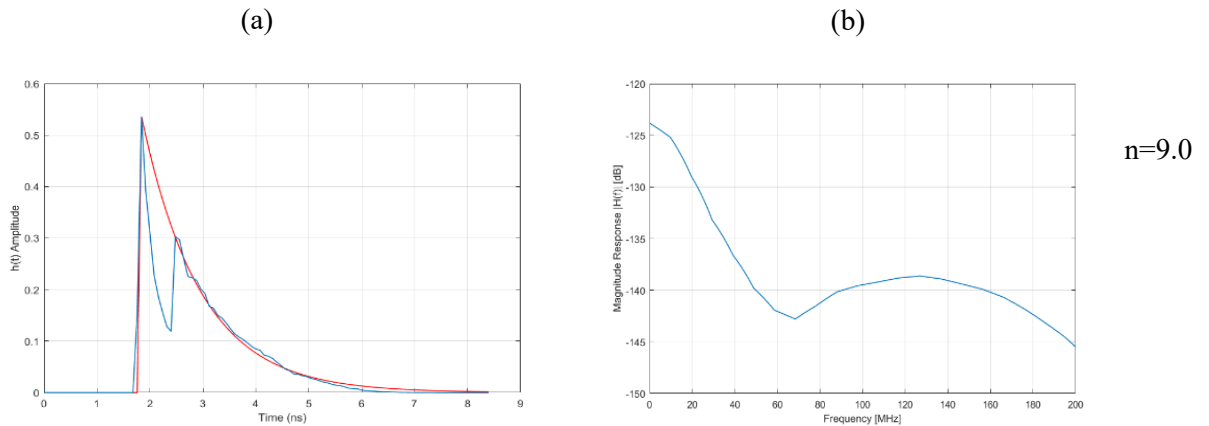(a)   (b)

n=8.6
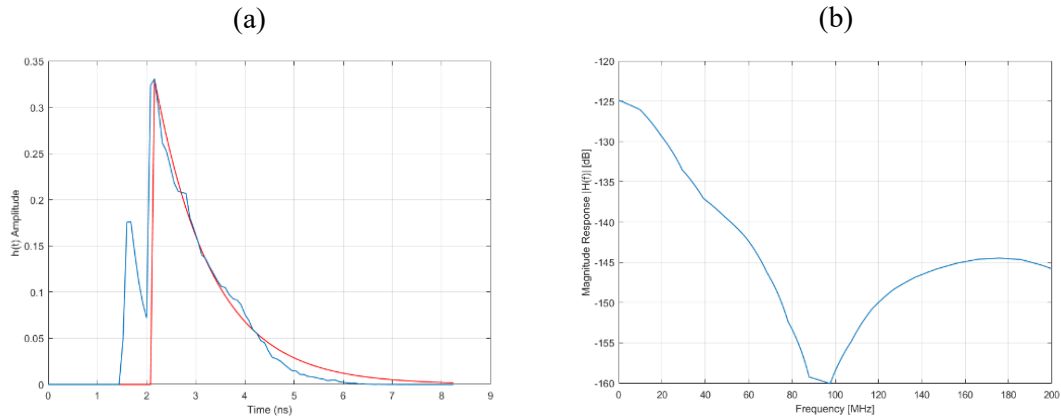
Fig. 40: Non-line-of-sight diffuse reflections (a) channel impulse response in time domain, (b) channel magnitude response in frequency domain simulated result (blue curve), approximation (red curve) for 30° elevation angle of transmitter. (a) indicates reflection of infrared signals from -90° azimuth angle of transmitter. For this case, first higher order reflection of impulse response is 0.33. The normalization of the impulse response that m equals to 8.7. (b) indicates the frequency response which is same power ratio with 90° azimuth angle at the lowest frequency.

3. SUMMARY

Device-to-device communication was studied in the simulation part. Empty room 5x5x3 m^3 was assumed, and reflection coefficient was taken into account the homogenous for each wall. Monte Carlo ray tracing method was used for NLOS VLC indoor environmental via MATLAB. Orientation of transmitter get involved significant role for each case.

First scenario of the transmitter is 5° elevation angle. Real scenario of a cell-phone user was assumed for this case. Second scenario of the transmitter is 30° elevation angle. The room conditions, movement of the user, reflection coefficient, field-of-view are the same in the Monte Carlo ray tracing method. The user is changing his orientation from 90° to -90° by 45° azimuth angle. The diffuse signal is distributed and reflected 3rd times from walls randomly. After the 3rd reflection, the detector is received the signal. Maximum impulse response which is high order reflection is at 0° angle. Moreover, it is the most important reflection that the result is ~30.8 dBm for both cases. Impulse response is ~-34.5 dBm at the 90° and -90° azimuth angle. There is approximately ~40dBm power loss after each reflection.

Transfer function is obtained by using Fourier transform. According to magnetic response is approximated by higher order low pass filter at under ~120 MHz/s. The second higher impulse response is observed from 45° and -45° angle and it is ~32 dBm. Obviously, power ratio is higher is at 0° angle and it is ~-134 dBm at 100MHz frequency for both situations. The exponential curve fitting value n directly proportional with the impulse response of the diffuse signal. If the n becomes high, the impulse response has better results for data transmission.

After the first high order reflection of the diffuse signal proceeds to become smooth. Therefore, exponential curve fitting is perfectly matching on the impulse response of the diffuse signal. Long decay has perfect effect on the low frequency part of the magnitude response of the diffuse signal. In a nutshell, the channel impulse response depends on the orientation of the transmitter and variable azimuth of transmitter.

4. CONCLUSION

In this diploma thesis, optical channel impulse response using Monte Carlo ray tracing method was observed via MATLAB. Moreover, BER performance of NLOS VLC link in indoor environment was investigated with reflection from different surfaces.

The first part of the diploma thesis, theoretical part was derived in details. Based on principle of VLC, modulation techniques were described and showned in block diagram. It was depicted link configuration of LOS and NLOS VLC. Reflection types and ray tracing models were explained and depicted.

The second part of the diploma thesis, measurement part was accomplished in the optical laboratory at Czech Technical University. White paper and black cotton material were used. During measurement, lab environment was completely dark to obtain precise results. The results show that, orientation of the transmitter and receiver is very significant on BER performance. Therefore, black cotton material has very high BER performance than white paper materal due to absorbtion feature. According to results, if transmitter`s angle is increased, lower BER performance is observed. Moreover, if bit number is increased, higher BER performance is observed. Obviously, there is direct proportion between number of subcarrier and BER performance.

The third part of the diploma thesis, simulation part was done in MATLAB using Monte Carlo ray tracing method to obtain channel impulse response. Rectangular homogenous empty room 5x5x3 m^3 was assumed. Orientation of the user-phone was precisely ensured. Also, real role of the user was taken into account for the $5°$ elevation angle of the transmitter in the simulation. The results show that $5°$ elevation angle has a better impulse response after the 3rd reflection than $30°$ elevation angle. The most important reflection was shown in first high order reflection peak. Afterwards, impulse response becomes very smooth. Hence, number of exponential curve 'n' perfectly suits on the graph of the impulse response. For the frequency response, low pass filter was used. Impulse response was utilized for the frequency response by Fourier transform. The effects of movement of the user was investigated. Modify the angle of the transmitter to obtain better result is adequate for indoor non-line-of-sight visible light communication.

REFERENCES

[1] Z. Ghassemlooy, L. Nero Alves, S. Zvanovec and M. Ali Khalighi, Visible Light Communications: Theory and Applications, CRC Press, 2017.

[2] Z. Ghassemlooy, W. Popoola, S. Rajbhandari, Optical Wireless Communications: System and Channel Modelling with MATLAB, CRC Press, 2012.

[3] S. Dimitrov, and H. Haas, *Principles of LED Light Communications: Towards Networked Li-Fi*. Cambridge: Cambridge University Press, 2015, doi:10.1017/CBO9781107278929.

[4] J. Wang, Z. Kang, N. Zou, "Research on indoor visible light communication system employing white LED lightings,".

[5] R. Sagotra, R. Aggarwal, "Visible Light Communication," in *International Journal of Engineering Trends and Technology*, 2013.

[6] H. Le Minh *et al*., "100-Mb/s NRZ Visible Light Communications Using a Postequalized White LED," in *IEEE Photonics Technology Letters*, vol. 21, no. 15, pp. 1063-1065, Aug.1, 2009. doi: 10.1109/LPT.2009.2022413.

[7] J. Vučić *et al*., "230 Mbit/s via a wireless visible-light link based on OOK modulation of phosphorescent white LEDs," *2010 Conference on Optical Fiber Communication (OFC/NFOEC), collocated National Fiber Optic Engineers Conference*, San Diego, CA, 2010, pp. 1-3.

[8] Y. Tanaka, T. Komine, S. Haruyama and M. Nakagawa, "Indoor Visible Light Transmission System Utilizing White Led Lights," IEICE Transaction on Communications vol. E86B, no.8, pp.2440-2454.

[9] N. Fujimoto and H. Mochizuki, "614 Mbit/s OOK-based transmission by the duobinary technique using a single commercially available visible LED for high-speed visible light communications," *2012 38th European Conference and Exhibition on Optical Communications*, Amsterdam, 2012, pp. 1-3. doi: 10.1364/ECEOC.2012.P4.03.

[10] H. Li, X. Chen, J. Guo, and H. Chen, "A 550 Mbit/s real-time visible light communication system based on phosphorescent white light LED for practical high-speed low-complexity application," Opt. Express 22, 27203-27213 , 2014.

[11] A. J. Mendez, V. J. Hernandez, R. M. Gagliardi and C. V. Bennett, "Design of optical pulse position modulation (PPM) translating receiver," *2009 IEEE LEOS Annual Meeting Conference Proceedings*, Belek-Antalya, 2009, pp.18-19. doi: 10.1109/LEOS.2009.5343490.

[12] K. Lee and H. Park, "Modulations for Visible Light Communications with Dimming Control," in *IEEE Photonics Technology Letters*, vol. 23, no. 16, pp. 1136-1138, Aug.15, 2011. doi: 10.1109/LPT.2011.2157676.

[13] J. Choi, E. Cho, Z. Ghassemlooy *et al*., "Visible light communications employing PPM and PWM formats for simultaneous data transmission and dimming," *in Optical and Quantum Electronics,* vol. 47, no. 3, pp. 561-574, 2015.

[14] B. Bai, Z. Xu, Y. Fan, "Joint LED Dimming and High Capacity Visible Light Communication by Overlapping PPM," *The 19th Annual Wireless and Optical Communications Conference (WOCC)* Shanghai, 2010.

[15] G. Stepniak, J. Siuzdak, P. Zwierko, "Compensation of a VLC Phosphorescent White LED Nonlinearity by Means of Volterra DFE," in *IEEE Photonics Technology Letters,* vol. 25, no. 16, 2013.

[16] G. Stepniak, L. Maksymiuk, J. Siuzdak, "1.1 GBIT/s white lighting LED-based visible light link with pulse amplitude modulation and Volterra DFE equalization," in *Microwave and Optical Technology Letters,* vol. 57, no. 7, 2015.

[17] N. Chi, M. Zhang. Y. Zhou and J. Zhao, "3.375-Gb/s RGB-LED based WDM visible light communication system employing PAM-8 modulation with phase shifted Manchester coding," in *Optics Express,* vol. 24, no. 19, 2016.

[18] T. Komine and M. Nakagawa, "Fundamental analysis for visible-light communication system using LED lights," in *IEEE Transactions on Consumer Electronics,* 2004.

[19] M. Grabner and V. Kvicera, "On the relation between atmospheric visibility and optical wave attenuation," *16th IST Mobile and Wireless Communications Summit,* pp. 1-5, 2007.

[20] D. O`Brien, L. Zeng, H. Le-Minh, G. Faulkner, *et al.,* "Short-range optical wireless communications: Technologies for the Wireless Future," **Wireless World Research Forum (WWRF),** vol. 2, pp. 277-296, 2006.

[21] Z. Lubin, D. O`Brien, H. Le-Minh, G. Faulkner, K. Lee, D. Jung, Y. Oh, E. Tae Won, "High data rate multiple input multiple output (MIMO) optical wireless communications using white led lighting," in **IEEE Journal on Selected Areas in Communications**, vol. 27, no. 9, pp. 1654-1662, December 2009.doi: 10.1109/JSAC.2009.091215.

[22] G. Cossu, W. Ali, R. Corsini and E. Ciaramella, "Gigabit-class optical wireless communication system at indoor distance (1.5 – 4 m)," in *Optics Express,* vol. 23, no. 12, pp. 15700-15705, 2015.

[23] G. Cossu, A. M. Khalid, P. Choudhury, R. Corsini and E. Ciaramella, "3.4 Gbit/s visible optical wireless transmission based on RGB LED," in *Optics Express,* vol. 20, no. 26, pp. B501-B506, 2012.

[24] X. Huang, S. Chen, Z. Wang, J. Shi, Y. Wang, J. Xiao and N. Chi, "2.0-Gb/s Visible Light Link Based on Adaptive Bit Allocation OFDM of a Single Phosphorescent White LED," in *IEEE Photonics Journal,* vol. 7, no. 5, pp. 1-8, 2015

[25] X. Huang, J. Shi, J. Li, Y. Wang and N. Chi, "A Gb/s VLC Transmission Using Hardware Preequalization Circuit," in *IEEE Photonics Technologhy Letters,* vol. 27, no. 18.

[26] H. Chun, S. Rajbhandari, G. Faulkner, D. Tsonev, E. Xie *et. al,* "LED Based Wavelength Division Multiplexed 10 Gb/s Visible Light Communications," in *Journal of Lightwave Technology*, vol. 34, no. 13, 2016.

[27] J. Li, Z. Huang, X. Liu, and Y. Ji, "Hybrid time-frequency domain equalization for LED nonlinearity mitigation in OFDM-based VLC systems," in *Optics Express,* vol. 23, no. 1, pp. 611, 2015.

[28] G. Cossu, A. M. Khalid, P. Choudhury, R. Corsini and E. Ciaramella, "2.1 Gbit/s Visible Optical Wireless Transmission," in *European Conference and Exhibition on Optical Communication (ECOC),* 2012.

[29] S. Rajbhandari, H. Chun, G. Faulkner, *et. al.,* "High-Speed Integrated Visible Light Communication System: Device Constraints and Design Considerations," in *IEEE Journal on Selected Areas in Communications,* vol. 33, no. 9, 2015.

[30] P. Chvojka, K. Werfli, P. A. Haigh, S. Zvanovec, Z. Ghassemblooy, M. R. Bhatnagar, "Multi-band carrier-less amplitude and phase modulation for VLC: An overview," in *2017 First South American Colloquium on Visible Light Communications (SACVLC),* Santiago, 2017, pp. 1-6.

[31] K. O. Akande, P. A. Haigh, and W. O. Popoola, "Joint Equalization and Synchronization for Carrierless Amplitude and Phase Modulation in Visible Light Communication," in *2017 13th International Wireless Communications and Mobile Computing Conference (IWCMC),* Valencia, 2017, pp. 876-881. doi: 10.1109/IWCMC.2017.7986401.

[32] P. Chvojka, K. Werfli, S. Zvanovec *et al.*, "On the m-CAP Performance with Different Pulse Shaping Filters Parameters for Visible Light Communications," in **IEEE Photonics Journal**, vol. 9, no. 5, pp. 1-12, Oct. 2017, Art no. 7906712. doi: 10.1109/JPHOT.2017.2749203.

[33] F. M. Wu, C. T. Lin, C. C. Wei *et al.*, "Performance Comparison of OFDM Signal and CAP Signal Over High Capacity RGB-LED-Based WDM Visible Light Communication," in **IEEE Photonics Journal**, vol. 5, no. 4, pp. 7901507-7901507, Aug. 2013, Art no. 7901507.

[34] M. Uysal, F. Miramirkhani, T. Baykas, N. Serafimovski, V. Jungnickel, "Lifi channel models office home manufacturing cell," in Group for Wireless Personal Area Networks (WPANs), 2015.

[35] T. Komine and M. Nakagawa, "A study of shadowing on indoor visible-light wireless communication utilizing plural white LED lightings," **1st International Symposium on Wireless Communication Systems, 2004.**, Mauritius, 2004, pp. 36-40. doi: 10.1109/ISWCS.2004.1407204.

[36] N. Hayasaka, T. Ito, "Channel modelling of nondirected wireless infrared indoor diffuse link," in *Electronics and Communications in Japan (Part I: Communications),* vol. 90, no. 6, 2007.

[37] S. Jivkova and M. Kavehrad, "Shadowing and blockage in indoor optical wireless communications," ***GLOBECOM '03. IEEE Global Telecommunications Conference (IEEE Cat. No.03CH37489)***, San Francisco, CA, 2003, pp. 3269-3273 vol.6.doi: 10.1109/GLOCOM.2003.1258840

[38] A. Yokoi, J. Son, "VLC channel measurement in indoor application," in *IEEE P802.15 Working Group for Wireless Personal Area Networks (WPANs),* 2008.

[39] C.R. Lomba, R .T. VaIadas, A.M.de Oliveira Duarte, "Experimental characterisation and modelling of the reflection of infrared signals on indoor surfaces,"in *IEE Proc.-Optoelectron.,* vol. j4.5, no. 3, 1998.

[40]V. Jungnickel, V. Pohl, S. Nönnig, C. von Helmolt, "A Physical Model of the Wireless Infrared Communication Channel," in *IEEE Journal on Selected Areas in Communications,* vol. 20, no. 3.

[41] M. I. Sakib Chowdhury, W. Zhang, M. Kavehrad, "Combined Deterministic and Modified Monte Carlo Method for Calculating Impulse Responses of Indoor Optical Wireless Channels," in *Journal of Lightwave Technology,* vol. 32, no. 18, 2014.

[42] C. Chen, D. Basnayaka, H. Haas, "Non-line-of-sight Channel Impulse Response Characterisation in Visible Light Communications," in *IEEE ICC 2016 - Optical Networks and Systems,* 2016.

[43] F. E. Nicodemus, J. C. Richmond, J. J. Hsia, I. W. Ginsberg, T. Limperis, "Geometrical Considerations and Nomenclature for Reflectance," pp. 40-44.

[44] http://www.raytracegroundup.com/downloads/Chapter25.pdf

[45] F. J. Lopez-Hernandez, R. Perez-Jimeniz and A. Santamaria, "Monte Carlo calculation of impulse response on diffuse IR wireless indoor channels," in ***Electronics Letters***, vol. 34, no. 12, pp. 1260-1262, 11 June 1998. doi: 10.1049/el:19980825.

[46] O. Gonzalez, S. Rodriguez, R. Perez-Jimenez, B. R. Mendoza and A. Ayala, "Error Analysis of the Simulated Impulse Response on Indoor Wireless Optical Channels Using a Monte Carlo-Based Ray-Tracing Algorithm ," in *IEEE Transactions on Communications,* vol. 53, no. 1, 2005.

[47] D. Wu, Z. Ghassemlooy, H. Le Minh, S. Rajbhandari, M. A. Khalighi, X. Tang, "Optimisation of Lambertian Order for Indoor Non-directed Optical Wireless Communication," in *1st International Workshop on optical Wireless Comms in China*, 2012.

[48] P. A. Haigh, A. Aguado, Z. Ghassemlooy, P. Chvojka, K. Werfli, S. Zvanovec, E. Ertunc, T. Kanesan, "Multi-Band Carrier-less Amplitude and Phase Modulation for Highly Bandlimited Visible Light Communications-Invited Paper," *2015 International Conference on Wireless Communications & Signal Processing (WCSP)*, Nanjing, 2015, pp. 1-5.

[49] F. Miramirkhani, M. Uysal, "Channel Modelling and Characterization for Visible Light Communications", 2015 IEEE.

[50] T. Komine and M. Nakagawa , "Performance evaluation on visible-light wireless communication system using white LED lightings," 9th IEEE Symp. Comput. Communication, 2004, vol. 1, pp. 258-263

[51] S. Long, M. A. Khalighi, M. Wolf, S. Bourennane, and Z. Ghassemlooy, "Channel characterization for indoor visible light communicatios," in Proc. IWOW, Sep. 2014, pp. 75-79.

[52] K. Lee, H. Park, J. R. Barry, "Indoor channel characteristics for visible light communications," IEEE Comm. Lett., vol. 15, no.2, pp. 217-219, Feb. 2011.